

# Constraints on evaporating primordial black holes from the AMS-02 positron data

Jia-Zhi Huang

*Institute of Theoretical Physics, Chinese Academy of Sciences, Beijing 100190, China.*

*University of Chinese Academy of Sciences, Beijing, 100190, China.*

Yu-Feng Zhou

*Institute of Theoretical Physics, Chinese Academy of Sciences, Beijing 100190, China.*

*University of Chinese Academy of Sciences, Beijing, 100190, China. and*

*School of Fundamental Physics and Mathematical Sciences,*

*Hangzhou Institute for Advanced Study, UCAS, Hangzhou 310024, China.*

*International Centre for Theoretical Physics Asia-Pacific, Beijing/Hangzhou, China.*

(Dated: April 8, 2025)

## Abstract

Cosmic-ray (CR) positrons are relatively rare due to their secondary origin and thus sensitive to exotic contributions. Primordial black holes (PBHs) with masses above  $\sim 5 \times 10^{14}$  g can be stable sources of CR positrons due to Hawking radiation. The energies of the evaporated positrons can increase significantly through scattering with the Galactic random magnetic fields during the propagation in the Galaxy, which is a generic feature in diffusive re-acceleration CR propagation models. We show that in well-constrained diffusive re-acceleration models, a significant portion of CR positron flux can enter the energy region of  $\mathcal{O}(\text{GeV})$ , and can be constrained by the current AMS-02 data. As an example, we show that in the Galprop+Helmod model for CR propagation in the Galaxy and heliosphere, an upper limit of  $f_{\text{PBH}} \lesssim 2.15 \times 10^{-4}$  at PBH mass  $2 \times 10^{16}$  g can be obtained, which improve the previous constraints from the Voyager CR all-electron data by around an order of magnitude.

## I. INTRODUCTION

Astrophysical and cosmological observations suggest that the dominant component of the matter in the present Universe is in the form of non-luminous dark matter (DM). In many particle physics models, DM consists of a new type of elementary particle beyond the Standard Model (SM) of particle physics, which may participate in non-gravitational interactions with baryonic matter, such as weakly interacting massive particles (WIMPs), sterile neutrinos and QCD axions (for recent reviews of these particle candidates, see e.g. [1–3]). Despite great experimental efforts in recent decades, so far there is no confirmed signals of particle DM from direct, indirect and collider DM search experiments.

Primordial black hole (PBH) is an alternative DM candidate which does not require any new physics beyond the SM [4, 5]. PBHs are believed to have formed after the inflation [6–10], and subsequently evolved through accretion, mergers, and Hawking radiation. Depending on the time of formation, the masses of PBHs can vary in a large range. In general, the initial mass  $M_{\text{PBH}}$  of a PBH should be close to the Hubble horizon mass at the production time  $t$ ,  $M_{\text{PBH}} \sim c^3 t / G \simeq 10^{15} (t / 10^{-23} \text{ s}) \text{ g}$ , where  $c$  is the speed of light and  $G$  is the Newton constant. For two typical formation time  $t$  of the Planck time  $t \sim 10^{-43} \text{ s}$  and the time just before the big-bang nucleosynthesis (BBN)  $t \sim 1 \text{ s}$ , the initial PBH mass are respectively around  $10^{-5} \text{ g}$  and  $10^5 M_{\odot}$ , where  $M_{\odot}$  is the mass of the Sun.

PBH can comprise all or a fraction of the DM. The energy fraction of PBHs relative to that of whole DM is defined as  $f_{\text{PBH}} \equiv \Omega_{\text{PBH}} / \Omega_{\text{DM}}$ , where  $\Omega_{\text{DM}}$  and  $\Omega_{\text{PBH}}$  are the energy density parameters of DM and PBHs relative to the critical density of the present Universe, respectively. For heavy PBHs with  $M_{\text{PBH}} \gg 10^{17} \text{ g}$ , the value of  $f_{\text{PBH}}$  can be constrained by the gravitational effects from PBHs such as microlensing [11–17], dynamical constraint from globular clusters, galaxy disruption and other observables [18–21] (for recent reviews, see e.g. [22, 23]).

Light PBHs are expected to emit SM particles through Hawking radiation [24]. PBHs in the mass range from  $10^{13} - 10^{17} \text{ g}$  are expected to emit SM particles with typical energies from a few GeV down to a few hundreds of keV. PBHs lose their masses through Hawking radiation at a rate  $dM_{\text{PBH}}/dt \propto M_{\text{PBH}}^{-2}$  [25, 26], which suggests that heavier PBHs evaporate slower. It has been shown that PBHs with masses  $M_{\text{PBH}} \gtrsim 5 \times 10^{14} \text{ g}$  have lifetimes larger than the age of the Universe, and can be considered as stable sources of photons and cosmic-ray (CR) particles in the Galaxy [27]. This type of evaporating PBHs can be searched by current space-borne experiments. For PBHs in this mass region, the value of  $f_{\text{PBH}}$  can be constrained by the data of extragalactic and galactic diffuse  $\gamma$ -rays [28–31], CMB [32], neutrinos [33–36], CR electrons [37], 511 keV gamma-ray lines [33, 38–40], 21-cm radio signals [41] and CR antiprotons [42, 43], etc.

The measured CR fluxes can also place importance constraints on  $f_{\text{PBH}}$ . Recently, low-energy CR all-electron ( $e^+ + e^-$ ) flux data from Voyager-1 have been used to set constraints on  $f_{\text{PBH}}$  [37]. The obtained limits turned out to be competitive with that derived from extragalactic  $\gamma$ -rays. As Voyager-1 is now outside the heliopause, the electron flux measured by Voyager-1 can be considered as the true local interstellar (LIS) flux, and the derived constraints are expected to be relatively

robust against the influence of the solar activity, the so called solar modulation effect. Note, however, that although the low-energy electron data from Voyager-1 can be considered as the true LIS flux, the theoretical prediction for CR flux from PBH evaporation involves a number of parameters for the CR propagation within the Galaxy, such as the diffusion coefficient, re-acceleration coefficient and convection velocity. These parameters are determined through fitting to the CR data (e.g the Boron to Carbon flux ratio, B/C) measured at the top of the atmosphere (TOA) deep inside the heliosphere, which are strongly affected by the solar activities. Thus, the constraints on the PBH fraction from the Voyager data are *inevitably* affected by the solar modulation effect. Actually, the LIS fluxes measured by Voyager-1, 2 are more useful in improving the modeling and calibrating of the solar modulation effect itself. In order to derive robust constraints on exotic contributions, it is necessary to consider both the LIS and TOA CR flux data simultaneously and consistently calculate the CR propagation in the Galaxy and heliosphere, as the parameters of the two processes are strongly correlated.

In this work we explore the possibility of using CR positron flux to constrain the abundance of PBHs. CR positrons are believed to be of secondary origin and relatively rare. Thus they are sensitive to exotic contributions. The low-energy CR positron flux can be used to set constraints on exotic contributions as they are roughly consistent with the expected backgrounds (see, e.g. [44]). Although the initial energy of the CR positrons from the PBHs with mass above  $5 \times 10^{14}$  g should be well below  $\mathcal{O}(10)$  MeV, the energies of final positrons can increase significantly through scattering with the Galactic random magnetic fields during the propagation process [45], which is a typical feature in many diffusive re-acceleration CR propagation models [46–53]. It has been shown that CR propagation plays an important role in constraining exotic contributions from CR data (see e.g. [54–57]). In this work, we show that in some well-constrained diffusive re-acceleration models, a significant portion of CR positrons can enter the GeV region, and can be constrained by the current AMS-02 experiment which can measure the CR positron flux with kinetic energy down to 0.6 GeV. We use the state-of-the-art models for CR propagation in the Galaxy (using the numerical code Galprop [58–62]) and in the heliosphere (using the numerical solutions of the Parker equation based on the Helmod code [63–67] and the analytical force-field approximation). In calculating the CR fluxes from PBH evaporation, we use the BlackHawk [68] code, which includes both the primary and secondary particle components. The results show that for typical diffusive re-acceleration models the AMS-02 positron data can provide very stringent limits, which can be stronger than the previous constraints derived from the Voyager all-electron flux by around an order of magnitude.

The remaining part of this paper is organized as follows. In section II, we give a brief overview on the positron energy spectrum from PBH evaporation. In section III, we discuss the CR propagation in the Galaxy and the models for solar modulation. The constraints on PBH abundances from the AMS-02 positron data are discussed in section IV for the cases without and with background included. The results of this work is summarized in section V.

## II. EVAPORATION OF PRIMORDIAL BLACK HOLES

In this work, unless otherwise stated, we adopt the natural system of units with  $\hbar = k_B = c = 1$ , where  $\hbar$  is the reduced Plank constant,  $k_B$  is the Boltzmann constant, and  $c$  is the speed of light. We consider a simple scenario where the spin of PBHs can be negligible, which can be obtained from a series of possible formation mechanisms [69–71] (for the formation of PBHs with near-extremal spin, see e.g. [72–74]). The emission rate of particle species  $i$  per unit time  $t$  and total energy  $E$  from Hawking radiation is given by [75]

$$\frac{d^2 N_i}{dt dE} = \frac{g_i \Gamma_i}{2\pi} \left[ \exp\left(\frac{E}{T_{\text{PBH}}}\right) - (-1)^{2s_i} \right]^{-1}, \quad (1)$$

where  $s_i$  and  $g_i$  are the spin and the total degree of freedom of the particle  $i$ , respectively, and the temperature  $T_{\text{PBH}}$  of a PBH with mass  $M_{\text{PBH}}$  is [76]

$$T_{\text{PBH}} \approx 10.6 \times \left( \frac{10^{15} \text{ g}}{M_{\text{PBH}}} \right) \text{ MeV}. \quad (2)$$

The graybody factor  $\Gamma_i$  in Eq. (1) is determined by the equation of motion of the particle in curved space time near the horizon. It describes the probability that the particle  $i$ , created at the PBH horizon, finally escapes to spatial infinity. In the geometric optics limit (i.e., the high-energy limit), the graybody factor for electron can be approximated as  $\Gamma_e \simeq 27 G^2 M_{\text{PBH}}^2 E^2$ . Note that Eq. (1) only describes the primary particles directly emitted from PBHs. The decays of the unstable primary particles can produce secondary stable particles. In the calculation of the graybody factor and the energy spectra of the emitted particles, we use the numerical code of BlackHawk [68, 77] in which both the primary and secondary production processes are calculated. For the low-energy particle production and decay, we use the results from the Hazma code [78] which is now included in the updated version BlackHawk-v2.1 [68].

The energy spectrum  $d^2 n_{e^\pm} / dt dE_{\text{kin}}$  from all the evaporating PBHs with different masses is given by

$$\frac{d^2 n_{e^\pm}}{dt dE_{\text{kin}}} = \int_{M_{\text{min}}}^{\infty} dM_{\text{PBH}} \frac{d^2 N_{e^\pm}}{dt dE_{\text{kin}}} \frac{dn}{dM_{\text{PBH}}}, \quad (3)$$

where  $dn/dM_{\text{PBH}}$  is the mass distribution function of PBH. Depending on formation mechanisms, the mass function can be a peak theory distribution [6, 7], log-normal distribution [8], monochromatic distribution [9] or power-law distribution [10]. In this work, we consider two widely used models, namely, monochromatic and log-normal mass functions. A nearly monochromatic mass function is naturally expected if all PBHs are formed at a same epoch, and a log-normal mass function can arise from inflationary fluctuations [79, 80]. The two mass functions are given by

$$\frac{dn}{dM_{\text{PBH}}} = \begin{cases} A_1 \delta(M_{\text{PBH}} - M_c) & \text{(monochromatic)} \\ \frac{A_2}{\sqrt{2\pi}\sigma M_{\text{PBH}}^2} \exp\left[-\frac{\ln^2(M_{\text{PBH}}/M_c)}{2\sigma^2}\right] & \text{(log-normal),} \end{cases} \quad (4)$$

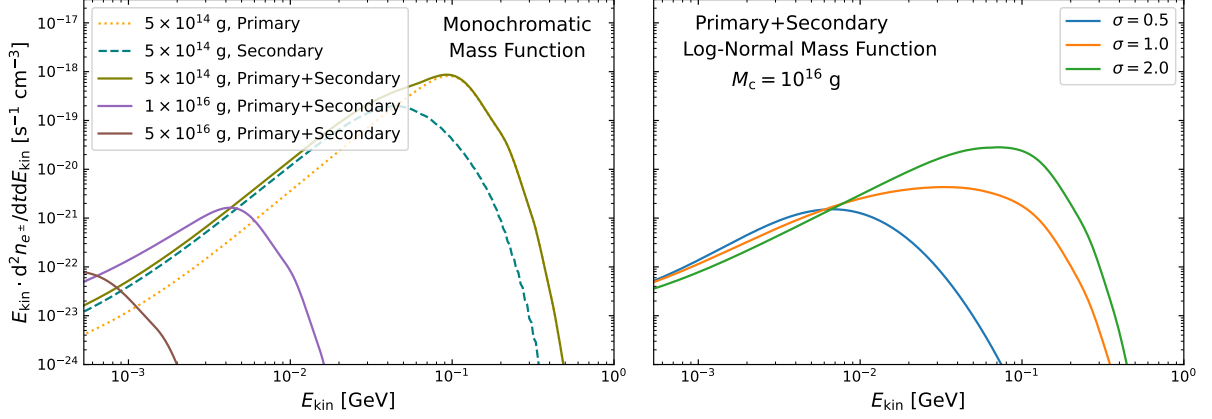


FIG. 1. Left) Initial fluxes of CR positron evaporated from PBHs with monochromatic mass distribution with  $M_c = 5 \times 10^{14}$  g,  $1 \times 10^{16}$  g, and  $5 \times 10^{16}$  g and energy density  $\rho_{\text{PBH}} = 0.43 \text{ GeV cm}^{-3}$ . For the case of light PBHs with  $M_c = 5 \times 10^{14}$  g, the contribution from the secondary positrons are also shown as they are non-negligible. Right) The same as the left but for log-normal mass distribution with  $M_c = 10^{16}$  g and three different widths  $\sigma = 0.5, 1.0$  and  $2.0$ .

where  $M_c$  is the characteristic mass,  $\sigma$  is the width of the log-normal mass distribution,  $A_1$  and  $A_2$  are normalized factors with different unit, which are determined by  $\rho_{\text{PBH}}$  the energy density of PBH as follows

$$\int_{M_{\min}}^{\infty} M_{\text{PBH}} \frac{dn}{dM_{\text{PBH}}} dM_{\text{PBH}} = \rho_{\text{PBH}}. \quad (5)$$

Due to Hawking radiation, PBHs continually lose their masses. Analytical and numerical calculations both confirmed that the lighter the PBH, the faster the evaporation [81, 82], suggesting PBHs with very small masses ( $\lesssim 5 \times 10^{14}$  g) are absent by now. In this work we only take into account the contribution from the existing PBHs, the lower bound  $M_{\min}$  in Eq. (5) is fixed at  $M_{\min} = 5 \times 10^{14}$  g. From Eq. (5), the relation between the normalized factor and  $\rho_{\text{PBH}}$  can be obtained. It is evident that  $A_1 = \rho_{\text{PBH}}/M_c$  for  $M_c > M_{\min}$ . The value of  $A_2$  can be expressed as  $A_2 = \rho_{\text{PBH}}/k(\sigma)$ , where  $k(\sigma) \equiv \int_{M_{\min}}^{\infty} \frac{dM_{\text{PBH}}}{\sqrt{2\pi\sigma} M_{\text{PBH}}} \exp[-\frac{\ln^2(M_{\text{PBH}}/M_c)}{2\sigma^2}]$ . For typical  $\sigma$  in the range 0.5-2.0, the value of  $k$  is found to be in the range  $0.5 \lesssim k \lesssim 1$  from numerical calculations. The case of  $k = 1$  corresponds to the limit of  $M_{\min} = 0$ .

In the left panel of Fig. 1, we show the calculated emission spectrum  $d^2 N_{e^\pm}/dt dE_{\text{kin}}$  for CR  $e^\pm$  as a function of kinetic energy  $E_{\text{kin}} = E - m_e$  in the monochromatically distributed PBHs with typical masses  $M_c = 5 \times 10^{14}$  g,  $1 \times 10^{16}$  g and  $5 \times 10^{16}$  g, respectively. For light PBHs with  $M_c = 5 \times 10^{14}$  g, the contributions from secondary particles are important, the secondaries can be dominant in the low-energy region below 10 MeV and can change the spectral shape significantly. For heavier PBHs with  $M_c \gtrsim 1 \times 10^{16}$  g, the secondary contribution is negligible, so only the total contribution is shown. In the right panel of Fig. 1, the energy spectra for the case of log-normal PBH mass distribution is shown for fixed  $M_c = 1 \times 10^{16}$  g with three different widths of  $\sigma = 0.5, 1.0$  and  $2.0$ . Compared with the left panel, for larger width such as  $\sigma = 2.0$ , the spectra can extend

to much higher energies, since the number density of lighter PBHs is significantly increase with given energy density  $\rho_{\text{PBH}}$ .

### III. CR PROPAGATION IN THE GALAXY AND THE HELIOSPHERE

#### A. CR propagation in the Galaxy

We use the two-dimensional (2D) diffusion models for CR propagation in the Galaxy. In our models, the diffusion zone is assumed to be a cylinder with radius  $R_h \approx 20$  kpc and half-height  $z_h = 1 \sim 10$  kpc [45, 83]. The diffusion equation of CR charged particles can be written as [45, 84]

$$\begin{aligned} \frac{\partial \psi}{\partial t} = & q(\mathbf{r}, p) + \nabla \cdot (D_{xx} \nabla \psi - \mathbf{V}_c \psi) + \frac{\partial}{\partial p} p^2 D_{pp} \frac{\partial \psi}{\partial p} \\ & - \frac{\partial}{\partial p} \left[ \dot{p} \psi - \frac{p}{3} (\nabla \cdot \mathbf{V}_c) \psi \right] - \frac{\psi}{\tau_f} - \frac{\psi}{\tau_r}, \end{aligned} \quad (6)$$

where  $\psi(\mathbf{r}, p, t)$  is the number density per unit of particle momentum  $p$  at the position  $\mathbf{r}$  which is related to the phase space distribution function  $f(\mathbf{r}, \mathbf{p}, t)$  as  $\psi(\mathbf{r}, p, t) = 4\pi p^2 f(\mathbf{r}, \mathbf{p}, t)$ ,  $q(\mathbf{r}, p)$  is the time-independent source term,  $D_{xx}$  is the energy-dependent spatial diffusion coefficient,  $\mathbf{V}_c$  is the convection velocity related to the galactic wind,  $D_{pp}$  is the diffusion coefficient in momentum space,  $\dot{p} \equiv dp/dt$  is the momentum loss rate,  $\tau_f$  and  $\tau_r$  are the time scales of particle fragmentation and radioactive decay, respectively. For the boundary conditions, it is assumed that particles can escape freely at the boundary of the diffusion halo. In cylinder coordinates, the boundary condition corresponds to  $\psi(R = R_h, z, p) = \psi(R, z = \pm z_h, p) = 0$ , where  $R$  and  $z$  are the cylinder radius and the height, respectively. For stable CR sources, the steady-state solution can be achieved, the corresponding condition is  $\partial \psi / \partial t = 0$ . The diffusion equation can be numerically solved use public codes, such as the Galprop code [58–62].

In the diffusion equation, the diffusion coefficient  $D_{xx}$  represents the CR scattering with the random magnetic fields, which can be parameterized as follows

$$D_{xx} = \beta^\eta D_0 \left( \frac{\rho}{\rho_0} \right)^\delta, \quad (7)$$

where  $\rho = p/(Ze)$  is the rigidity of the CR particle with electric charge  $Ze$ ,  $D_0$  is a normalization constant determined at a reference rigidity  $\sim 4$  GV,  $\delta$  is the spectral power index, for Kolmogorov type of turbulence  $\delta = 1/3$  [85], and for an Iroshnikov-Kraichnan cascade  $\delta = 1/2$  [86, 87],  $\beta = v/c$  is the velocity of CR particles relative to the speed of light  $c$ , and  $\eta$  is a parameter introduced to accommodate the low-rigidity behavior of the CR spectra. If necessary, *ad hoc* breaks in the power-law behavior in rigidity can be introduced. For instance, in one-break case,  $\delta$  can take two different values of  $\delta_{0(1)}$  for  $\rho$  below (above) a reference rigidity  $\rho_0$ . For multiple breaks,  $\delta$  can take different values of  $\delta_i$  in the rigidity region  $\rho_{i-1} \leq \rho \leq \rho_i$ , where  $\rho_i$  are the corresponding reference rigidities.

The diffusion in momentum space is described by the parameter  $D_{pp}$  which can be parameterized as follows [45, 88]

$$D_{pp} = \frac{4V_a^2 p^2}{3D_{xx} \delta (4 - \delta^2)(4 - \delta)}, \quad (8)$$

where  $V_a$  is the Alfvén velocity which characterizes the propagation of disturbances in Galactic magnetic fields. The scattering of charged particles by the random motion of the magnetic fields characterized by the Alfvén velocity leads to a certain amount of second-order Fermi acceleration during propagation, which can significantly modify the low-energy CR spectra.

In this work the value of  $V_a$  is considered to be constant in the whole diffusion halo, which should be understood as an effective parameter. In some semi-analytic framework, the re-acceleration is assumed to be confined in the galactic disk normalized to a half-width of  $h \sim 0.1$  kpc, which allows for fast analytical calculations for CR propagation (see e.g. [89]). The value of  $V_a$  obtained in the semi-analytical approach should be roughly rescaled by a factor of  $\sqrt{h/z_h}$  when compared with the one adopted in this work.

The convection velocity  $\mathbf{V}_c$  is modeled as a vector field perpendicular to the galactic disk, starting from  $V_{c0}$  at  $z = 0$  and increases linearly with  $z$  with gradient  $dV_c/dz$ . The expression is  $\mathbf{V}_c = \hat{\mathbf{e}}_z(V_{c0} + (dV_c/dz) \cdot |z|) \cdot z/|z|$ , where  $\hat{\mathbf{e}}_z$  is the unit vector alongside the direction of the  $z$  axis.

CR electrons/positrons loss energy through the process of ionization, Coulomb scattering, bremsstrahlung in the neutral and ionized medium, and also through synchrotron radiation and inverse Compton scattering (ICS). For the kinetic energy below GeV, the energy loss is dominated by ionization, Coulomb scattering. Above GeV, the energy loss is dominated by synchrotron radiation and ICS processes [58, 90]. The atomic hydrogen (HI) distribution is represented by  $n_{\text{HI}}(R, z) = n_{\text{HI}}(R) \exp[-2 \ln 2(z/z_0)^2]$ , where  $n_{\text{HI}}(R)$  and  $z_0$  are taken from [91, 92]. The distribution of molecular hydrogen ( $\text{H}_2$ ) is taken as  $n_{\text{H}_2}(R, z) = n_{\text{H}_2}(R) \exp[-2 \ln 2(z/70\text{pc})^2]$  from CO surveys and  $n_{\text{H}_2}(R)$  is from [93]. The distribution of the ionized gas (HII) is taken as the two-component model from [94]. The interstellar radiation field (ISRF) is relevant for the leptonic energy losses via ICS process. The low-energy photons involved in this process originate from stars, and are further reprocessed by Galactic dust; CMB photons also contribute with a comparable energy density. In the Galprop code, the ISRF calculation uses emissivities based on stellar populations and dust emission. The infrared emissivities per atom of HI,  $\text{H}_2$  are based on COBE/DIRBE data from [95], combined with the distribution of HI and  $\text{H}_2$ .

The primary CR electrons are believed to be accelerated by supernova remnants (SNR) and pulsar wind nebulae. The distribution of the primary CR sources can be modeled by a spatial density function multiplied by a broken power-law spectrum with  $m$ -fold breaks at rigidities  $\rho_i$ , ( $i = 1, \dots, m$ ) with indices  $\gamma_i$  before each break

$$q(\mathbf{r}, p) = n(\mathbf{r}) \left( \frac{\rho}{\rho_0} \right)^{-\gamma_0} \prod_{i=0}^{m-1} \left[ \frac{\max(\rho, \rho_i)}{\rho_i} \right]^{\gamma_i - \gamma_{i+1}}. \quad (9)$$



For instance, if only one break at  $\rho_0$  is considered, the source power term has two power indices  $\gamma_0$  and  $\gamma_1$ . The spatial distribution of the primary sources is assumed to follow that of SNRs, which is parameterized as follows

$$n(R, z) \propto \left(\frac{R}{r_\odot}\right)^a \exp\left(-b\frac{R - r_\odot}{r_\odot}\right) \exp\left(-\frac{|z|}{0.2 \text{ kpc}}\right), \quad (10)$$

where the two source parameters  $a$  and  $b$  slightly depends on CR species.

In addition to the primary CR electrons, there are secondary CR  $e^\pm$  created by the collision of primary CR nuclei with the interstellar medium (ISM). The secondary source term for CR electrons and positrons is given by

$$q_{e^\pm}^{\text{sec}}(\mathbf{r}, p) = \sum_{ij} n_j(\mathbf{r}) \int dp_i c \beta_i \psi_i(\mathbf{r}, p_i) \frac{d\sigma^{ij \rightarrow e^\pm}(p, p_i)}{dp}, \quad (11)$$

where the index  $i$  runs through primary CR particles such as proton and Helium,  $\beta_i$  is the velocity of primary CR particle  $i$ ,  $n_j$  is the number density of the  $j$ -th ISM component with  $j$  runs through HI, HII, and H<sub>2</sub>,  $d\sigma^{ij \rightarrow e^\pm}(p, p_i)/dp$  is the differential cross-section for creating a secondary  $e^\pm$  with momentum  $p$  from an incident primary particle  $i$  with momentum  $p_i$ . Secondary  $e^\pm$  are typically produced from the decay of  $\pi^\pm$  and  $K^\pm$  during the collision with ISM [90].

## B. CR propagation in the Heliosphere

In the vicinity of the Sun, the propagation of charged CR particles is affected by the regular and irregular heliospheric magnetic fields generated by the out flowing solar wind. The solar activity leads to time-dependent suppression of the CR particle flux with rigidity below  $\sim 50$  GV, which is referred to as the solar modulation effect. In this work we consider two approaches for estimating the solar modulation effect. One is based on numerical solution of the Parker equation, the other one is based on the force-field approximation.

### 1. The Parker equation

The CR propagation in the heliosphere can be described by the following Parker equation

$$\frac{\partial U}{\partial t} = \nabla \cdot (K^S \nabla U - (\mathbf{V}_{\text{sw}} + v_d)U) + \frac{1}{3} \nabla \cdot \mathbf{V}_{\text{sw}} \frac{\partial}{\partial T} (\alpha_{\text{rel}} E_{\text{kin}} U), \quad (12)$$

where  $U(\mathbf{r}, t, E_{\text{kin}})$  is the particle number density per kinetic energy  $E_{\text{kin}}$ ,  $K^S$  is the symmetric part of the diffusion tensor,  $V_{\text{sw}}$  is the solar wind velocity,  $v_d$  is the particle magnetic drift velocity, and  $\alpha_{\text{rel}} = (E_{\text{kin}} + 2m)/(E_{\text{kin}} + m)$ . The component of  $K^S$  parallel to the magnetic field  $K_{\parallel}$  is believed to be dominant over that perpendicular component  $K_{\perp}$ . The parallel component is parametrized as

$$K_{\parallel} = \frac{\beta}{3} K_0 \left( \frac{\rho}{1 \text{ GV} + g_{\text{low}}} \right) \left( 1 + \frac{r}{1 \text{ AU}} \right), \quad (13)$$



where  $K_0$  is the diffusion parameter and  $r$  is the distance to the Sun,  $g_{\text{low}}$  is a parameter depends on the solar activity. The  $i$ -th perpendicular component  $K_{\perp,i}$  is related to the parallel component through  $K_{\perp,i} = \rho_i K_{\parallel}$ . The parameters  $g_{\text{low}}$  and  $\rho_i$  are two major free parameters which need to be determined by the CR data measured at different periods of solar activity. The Parker equation can be numerically solved using the code `Helmod` [63–67] in which the propagation parameters are calibrated using the up-to-date CR data. In the `Helmod` code, the CR flux at TOA is related to that in the LIS as follows

$$\Phi^{\text{TOA}}(\rho) = \int \Phi(\rho) G(\rho, \rho') d\rho', \quad (14)$$

where  $G(\rho, \rho')$  is the normalized probability for a CR particle with a rigidity  $\rho'$  in the LIS but observed at TOA with a rigidity  $\rho$ . The function  $G(\rho, \rho')$  can be obtained from the `Helmod` python module which provides the numerical values with rigidity binning and time interval according to the given CR measurements. The `Helmod` code is able to quantitatively reproduce the time variation of CR fluxes such as that of protons, and the predicted LIS proton flux is in remarkable agreement with the Voyager-1 data [66]. Other numerical codes solving the Parker equation include `SOLARPROP` [96] and `HELIOPROP` [97], etc.

## 2. Force field approximation

Another commonly-adopted model for solar modulation is based on the simplified force-field approximation [98]. In this approach, the CR flux  $\Phi$  at TOA is related to that at LIS through the relation

$$\Phi^{\text{TOA}}(E_{\text{kin}}^{\text{TOA}}) = \left( \frac{2mE_{\text{kin}}^{\text{TOA}} + (E_{\text{kin}}^{\text{TOA}})^2}{2mE_{\text{kin}} + E_{\text{kin}}^2} \right) \Phi(E_{\text{kin}}). \quad (15)$$

The kinetic energy  $E_{\text{kin}}$  of the CR particle in LIS is related to that at TOA through the relation  $E_{\text{kin}} = E_{\text{kin}}^{\text{TOA}} + e\phi_F|Z|$ , where  $\phi_F$  is the so-called Fisk potential which is a phenomenological parameter that needs to be determined together with other propagation parameters. In this method, the solar modulation effect is assumed to be homogeneous. The value of  $\phi_F$  is dependent on the CR species, and different values of  $\phi_F$  should be adopted to fit the same CR specie measured at different time period. There is a strong degeneracy between  $\phi_F$  and the CR propagation parameters and the primary source parameters.

## C. Benchmark propagation models

As shown in Eq. (8), re-acceleration is generically linked to the spatial diffusion of CR particles, and has important phenomenological consequences. It is known that re-acceleration can provide a natural mechanism to reproduce the low-energy B/C ratio with Kolmogorov type of turbulence and a spectral break in the power-law spectrum of primary CRs at a rigidity of few GV [99]. Currently,

diffusive re-acceleration models with a sizable  $V_a \sim 30$  km/s has received strong support from a number of independent analyses [46–53]. For instance, a global fit to the B/C and Carbon data from HEAO-3, ACE and ATIC-2 using the Galprop with force-field approximation for solar modulation found  $V_a = 38.4 \pm 2.1$  km/s [46]. Similar updated analysis using the AMS-02 proton and B/C data gave  $V_a = 44.6 \pm 1.2$  km/s [47]. A recent analysis including the AMS-02 data of Be, B, C, N, O nuclei also favored a large  $V_a = 30 \pm 2.5$  km/s [100]. It was also noticed that fit to another data set of proton, antiproton and Helium tended to give a smaller value of  $V_a$ , which suggest that different CR species may explore different parts of the ISM [100]. In an analyses used the Helmod code for calculating the solar modulation, fitting to the AMS-02 B/C, proton and He data gave  $V_a = 28.6 \pm 3$  km/s [49]. The result was confirmed by the updated analyses including more secondaries such as Be and Li [50, 51]. For the analyses using the numerical code Dragon for CR propagation, a recent analysis considered a set of cross sections for the production of secondaries [52] which are different from those adopted by the Galprop code, and found  $V_a \sim 30$  km/s from fitting to the AMS-02 data of B/C, B/O, Li/C, Li/O flux ratios [53].

Since the effects of different propagation parameters and the injection spectrum are partially degenerated, it is possible to construct alternative propagation models without re-acceleration but include more complicated energy dependence in the diffusion term. A known example is to introducing an additional break in rigidity-dependent diffusion coefficient  $D_{xx}$  at rigidity around 4 GV and assuming  $V_a = 0$ . This type of diffusion break (DB) models can reproduce the similar structure in B/C flux ratio. So far both scenario can well explain the data of secondary/primary flux ratio [101–103]. Note that it is possible to distinguish the two scenarios in future by considering additional observables. For instance, the existence of  $V_a$  can be probed by synchrotron radiations [104] and a break in the injection primary source can be examined by gamma-ray emission from gas clouds [105].

In this work, we consider a number of Galprop-based propagation models with different methods for solar modulation calculations. We focus on the models with constant  $V_a$ . In the generic case,  $V_a$  is expected to be spatial dependent, as  $V_a \propto B/\sqrt{n_{\text{ISM}}}$  where  $B$  is the interstellar magnetic field and  $n_{\text{ISM}}$  is the number density of the ISM atoms. Since we are focused on CR positrons which cannot propagate to a long distance due to fast energy losses, we assume  $V_a$  to be a effective constant in the whole propagation halo.

- **GH-model.** In this model, we take the analysis framework of Galprop+Helmod (GH) where the two numerical codes Galprop and Helmod are combined together to provide a single framework to calculate CR fluxes at different modulation levels and at both polarities of the solar magnetic field [49–51, 106]. This is achieved by an iterative optimization procedure to tune the parameters in both Galprop and Helmod to best reproduce the data set of CR proton flux measured by PAMELA, BESS and AMS-02. The predicted LIS proton spectrum is in a remarkable agreement with the Voyager-1 data [66]. We adopt the parameters determined in [51] which is obtained by a Markov Chain Monte Carlo (MCMC) scan of the parameter space to fit the AMS-02 data of light nuclei. In this model, the best fit halo height is fixed at

$z_h = 4$  kpc, and the best-fit gradient of the convection velocity is  $dV_c/dz = 9.8 \text{ km s}^{-1} \text{ kpc}^{-1}$  with  $V_{c0} = 0$ . The diffusion coefficient follows a single power law, i.e.,  $\delta_0 = \delta_1 = 0.415$ . The injection primary spectra have two low-rigidity breaks located at  $\sim 1$  GV and  $\sim 7$  GV, respectively, which depend on CR species. For protons,  $\gamma_{0(1)}=2.24$  (1.70),  $\rho_{0(1)}=0.95$  (6.97), and for  ${}^6\text{C}$ ,  $\gamma_{0(1)}=1.00$  (1.10),  $\rho_{0(1)}=1.98$  (6.34). The details on the primary spectra for different species can be found in Table 2 of Ref. [51]. In this model, the source distribution parameters in Eq. (10) are fixed at  $a = 1.9$  and  $b = 5.0$ , respectively.

- **MIN-, MED-, MAX- and MAX2-models.** In this type of models, the simplified force-field approximation of Eq. (15) for solar modulation is adopted, which allows for fast analytical calculations of TOA fluxes and more flexibility to adjust model parameters in data fitting processes. In order to investigate the uncertainties in  $z_h$  due to the well-known  $z_h - D_0$  degeneracy, we first consider three propagation models from our previous analysis to the AMS-02 proton and B/C data [47], the so called MIN, MED and MAX models for Galprop with  $z_h = 1.8, 3.2$  and  $6$  kpc, respectively. The parameters in the models are slightly tuned to better reproduce the latest AMS-02 B/C 2021 data [107]. In addition, we also include a model with  $z_h = 10$  kpc (MAX2 model) which is derived from the MAX model. In all these models, the convection effect is not considered (i.e.,  $dV_c/dz = 0$  and  $V_{c0} = 0$ ), and the power index of the diffusion coefficient is close to the Kolmogorov type  $\delta_0 = \delta_1 \sim 0.3$ . The Fisk potential is fixed at  $\phi_F = 550$  MV. The CR primary spectra are assumed to have the same power-law index as that of CR protons which has a break at a reference rigidity  $\rho_0 = 4$  GV with  $\gamma_{0(1)} = 1.79$  (2.45) for the MED model. In these models, the values of the source parameters  $a = 1.25$  and  $b = 3.56$  are adopted, which are the default values in the Galprop code.
- **DB-model.** In this model, the re-acceleration term is switched off, i.e.  $V_a = 0$ , while a break in the diffusion coefficient  $D_{xx}$  is introduced at rigidity  $\bar{\rho}_0 = 3.94$  GV with two different diffusion power-law indices  $\delta_{0(1)} = -0.98$  (0.49). There is also no break assumed in the injection spectrum, i.e.,  $\gamma_0 = \gamma_1 = 2.4$ . The propagation parameters are based on the “BASE” propagation model proposed in [101]. In this model, the convection velocity is assumed to be constant  $V_{c0} = 3.34$  km/s with  $dV_c/dz = 0$ . The force-field approximation is adopted with the Fisk potential fixed at  $\phi_F = 610$  MV. For simplicity, the nuclear cross sections for the secondary production are taken as the default values in the Galprop code. Although in this work we focus on the re-acceleration models, this model serves as a useful counterexample.

The details of the parameters of these propagation models are listed in Tab. I. In the left panel of Fig. 2 we show the predicted B/C flux ratio from the six propagation models and compare them with the latest AMS-02 data [107]. The figure indicates that although the parameter sets are quite different, all of them can well explain the current data.

The source term for electrons and positrons from PBHs can be obtained by combining Eq. (3),

| Parameters  | GH    | MIN  | MED  | MAX  | MAX2 | DB    |
|---|-------|------|------|------|------|-------|
| $z_h$ [kpc]   | 4.0   | 1.8  | 3.2  | 6.0  | 10.0 | 4.0   |
| $D_0$ [ $10^{28}$ cm <sup>2</sup> s <sup>-1</sup> ] | 4.3   | 3.2  | 5.8  | 9.8  | 13.9 | 5.05  |
| $\eta$  | 0.7   | 1    | 1    | 1    | 1    | 1     |
| $\delta_0$  | —     | —    | —    | —    | —    | -0.98 |
| $\delta_1$  | 0.415 | 0.30 | 0.29 | 0.29 | 0.29 | 0.49  |
| $\bar{\rho}_0$ [GV]                                 | —     | —    | —    | —    | —    | 3.94  |
| $V_a$ [km s <sup>-1</sup> ]                         | 30    | 38   | 38   | 36   | 36   | —     |
| $\phi_F$ [GV]                                       | —     | 0.55 | 0.55 | 0.55 | 0.55 | 0.61  |
| $\gamma_0$  | 2.24  | 1.75 | 1.79 | 1.81 | 1.81 | 2.36  |
| $\gamma_1$  | 1.70  | 2.44 | 2.45 | 2.46 | 2.46 | —     |
| $\rho_0$ [GV]                                       | 0.95  | 4.0  | 4.0  | 4.0  | 2.5  | —     |

TAB. I. Fixed parameters for six CR propagation models GH [51], MIN, MED, MAX [47], MAX2 and DB. The primary indices  $\gamma_{0,1}$  and break rigidity  $\rho_0$  are for CR protons.  $\bar{\rho}_0$  is the rigidity break in diffusion coefficient  $D_{xx}$  in the DB model.

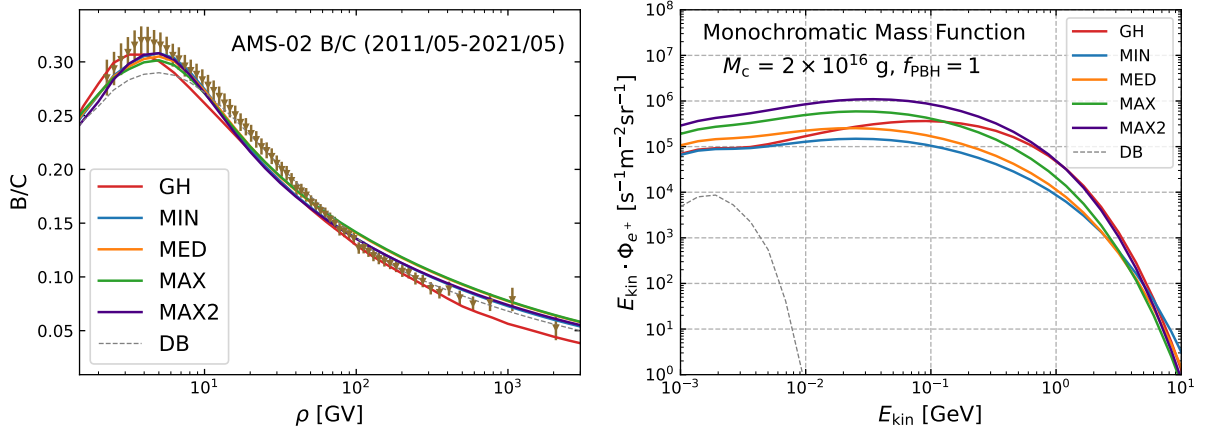


FIG. 2. Left) Boron to Carbon flux ratio in the six models listed in Tab. I. The data measured by the AMS-02 in the period 2011-2021 are shown for comparison. Right) Positron fluxes from PBH evaporation in the six propagation models. The PBH abundance is fixed at  $f_{\text{PBH}} = 1$  and mass function is assumed to be monochromatic with  $M_c = 2 \times 10^{16}$  g.

Eq. (5) and the PBHs spatial distribution in the Galaxy. For simplicity, the spatial distribution of PBHs is assumed to follow that of DM, namely,  $\rho_{\text{PBH}}(r)$  satisfies  $\rho_{\text{PBH}}(r) = f_{\text{PBH}} \cdot \rho_{\text{DM}}(r)$ , where  $\rho_{\text{DM}}(r)$  is the DM density profile. In this work, we adopt the Navarro-Frenk-White (NFW) profile [108]

$$\rho_{\text{DM}}(r) = \rho_0 \left(1 + \frac{r_\odot}{r_s}\right)^2 \left(\frac{r}{r_\odot}\right)^{-1} \left(1 + \frac{r}{r_s}\right)^{-2}, \quad (16)$$

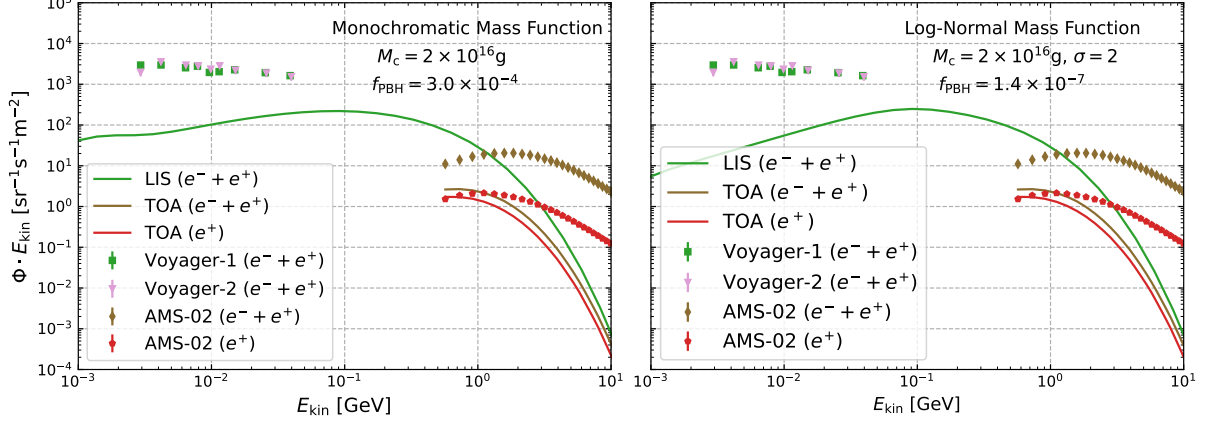


FIG. 3. Left) LIS and TOA CR positron and all-electron fluxes from the evaporation of PBHs in the GH propagation model. The PBH mass distribution is taken to be monochromatic with  $M_c = 2 \times 10^{16}$  g. The data of Voyager-1,2 (all-electron) [109] and AMS-02 (positron and all-electron) [110] are also shown. The value of  $f_{\text{PBH}}$  is chosen to saturate the AMS-02 positron data at lowest kinetic energy at 0.5 GeV. For the LIS (TOA) fluxes,  $E_{\text{kin}}$  represents the kinetic energy of CR particles at LIS (TOA). Right) The same as the left but for PBH log-normal mass distribution with  $M_c = 2 \times 10^{16}$  g and  $\sigma = 2.0$ .

where  $\rho_0 = 0.43 \text{ GeV} \cdot \text{cm}^{-3}$  is the local DM energy density,  $r_\odot = 8.5 \text{ kpc}$  is the distance of the Sun to the Galactic center, and  $r_s = 20 \text{ kpc}$  is a typical radius parameter. Note that the dependence of CR electron and positron fluxes on the DM profile is rather weak. In the right panel of Fig. 2, we show the predicted positron energy spectra for a monochromatic PBH distribution with a typical mass  $M_c = 2 \times 10^{16}$  g in the six propagation models. It can be seen that after calibrated by the B/C flux ratio, all the five models with re-acceleration predict similar positron spectra: a significant portion of the evaporated positrons can be boosted to GeV region, which suggest that the AMS-02 positron data can provide useful constraints. An exception is the DB model, in this model, the positron flux drops rapidly towards higher energies and features a cut off at  $\mathcal{O}(\text{MeV})$  as suggested by Eq. (2). Thus in this case the AMS-02 positron data cannot place useful constraints on  $f_{\text{PBH}}$ . In this type of models, the constraints can only be obtained from the Voyager all-electron data as previously discussed in [109].

In the left panel of Fig. 3, we show the CR positron and all-electron ( $e^- + e^+$ ) fluxes predicted from the evaporation of PBHs with monochromatic mass distribution at  $M_c = 2 \times 10^{16}$  g in the GH propagation model together with the data of AMS-02 (positron and all-electron) and Voyager-1, -2 (all-electron). In the figure we only show the predictions of the TOA flux in the same energy region as that of the published AMS-02 data, as the probability function  $G(\rho, \rho')$  provided by Helmod is specific for each experiment and data taking period. The astrophysical background electrons and positrons are not shown for the moment, such that conservative constraints (i.e. the constraints without including the astrophysical backgrounds) on  $f_{\text{PBH}}$  can be roughly inferred from comparing the theoretical predictions with the data. It can be seen that in the propagation model

under consideration, the PBH generated positron flux will be first constrained by the AMS-02 positron data in the GeV region rather than that from the Voyager all-electron data in the MeV region. Since the predicted CR fluxes depend on  $f_{\text{PBH}}$  linearly, we find by gradually increasing the value of  $f_{\text{PBH}}$  that for  $f_{\text{PBH}} \approx 3 \times 10^{-4}$  the predicted positron flux can saturate the low-energy positron flux at  $\sim 0.5$  GeV measured by AMS-02, which will set the scale of the final constraints from a more robust statistic analysis. We find similar results for other propagation models such as the MIN, MED, MAX and MAX2 models. In the right panel of Fig. 3, we show the result for the log-normal PBH mass function with  $M_c = 2 \times 10^{16}$  g and width  $\sigma = 2$  in the propagation model GH. The CR backgrounds are also neglected as that in the right panel. It can be seen that in this extended mass function the value of  $f_{\text{PBH}}$  will again be constrained first by the AMS-02 low-energy positron data. A typical constraint is at the level of  $f_{\text{PBH}} \lesssim 1.4 \times 10^{-7}$ .

At present, although the re-acceleration process is generally expected, the exact value of  $V_a$  is not yet conclusive. Fig. 3 suggests that if a large  $V_a$  of  $\sim 30 \text{ km} \cdot \text{s}^{-1}$  is confirmed by the future studies, the AMS-02 positron data will be more powerful in constraining  $f_{\text{PBH}}$  than the Voyager and AMS-02 all-electron data.

#### IV. CONSTRAINTS ON THE PBH ABUNDANCE

In this section, we derive the constraints on  $f_{\text{PBH}}$  from the current CR electron and positron data.

##### A. Constraints without including astrophysical backgrounds

In the first step, we derive the constraints under the assumption of null astrophysical backgrounds, which should be conservative and robust. In calculating the constraints, we adopt a simple approach by requiring that the predicted CR flux from PBH evaporation should not exceed the experimental data by more than  $2\sigma$  uncertainty in any energy bin, which was the approach adopted in Ref. [37], and thus allows for a direct comparison with their results. The constraints are obtained by simply rescaling the value of  $f_{\text{PBH}}$  and compare the predictions with the experimental data.

In Fig. 4, we show the obtained constraints on  $f_{\text{PBH}}$  in the six propagation models from the individual data set of Voyager-1, -2 all-electron, AMS-02 all-electron, and AMS-02 positron for monochromatically distributed PBHs with characteristic mass  $M_c$  in the range  $5 \times 10^{14} - 10^{17}$  g. It can be seen that for the GH, MIN, MED, MAX and MAX2 models, the constraints from the low-energy AMS-02 positron data are the most stringent. As an example, in the GH propagation model, we obtain conservative upper limit of

$$f_{\text{PBH}} \lesssim 2.15 \times 10^{-4} \text{ at } M_{\text{PBH}} = 2 \times 10^{16} \text{ g},$$

which is more stringent than that from the Voyager all-electron data by an order of magnitude. The AMS-02 positron constraints are also more stringent than that from the AMS-02 all-electron data. The reason is that the initial spectra of electrons and positrons from PBH evaporation are

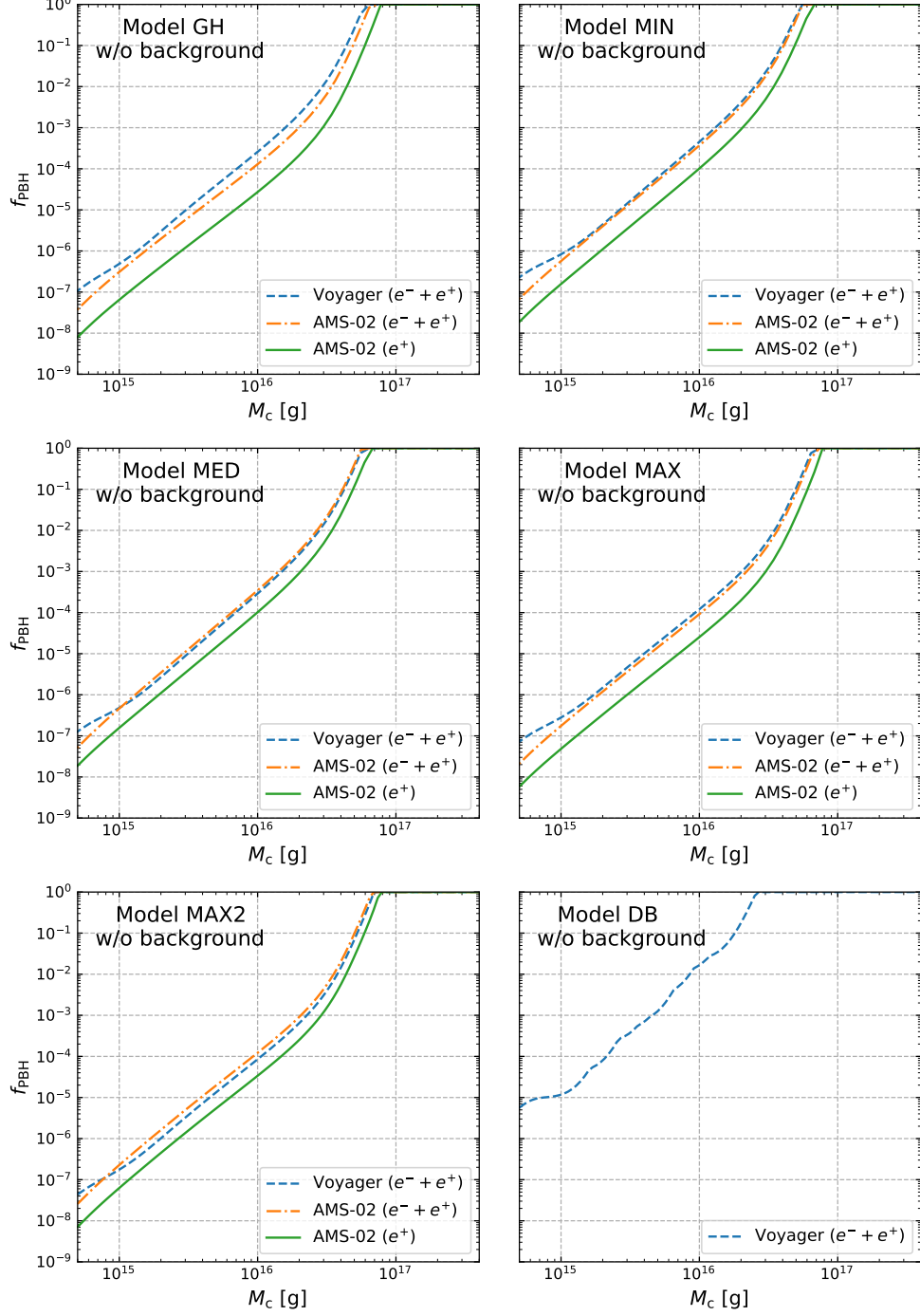


FIG. 4. Constraints on  $f_{\text{PBH}}$  in six CR propagation models as functions of the characteristic mass  $M_c$  of the monochromatic mass distribution. The parameters of the propagation models are listed in Tab. I. The solid-green, dashed-blue, and dot-dashed orange curves represent the constraints obtained individually from the positron data of AMS-02 [110], the all-electron data of Voyager-1,2 [109] and the all-electron data of AMS-02 [110], respectively.



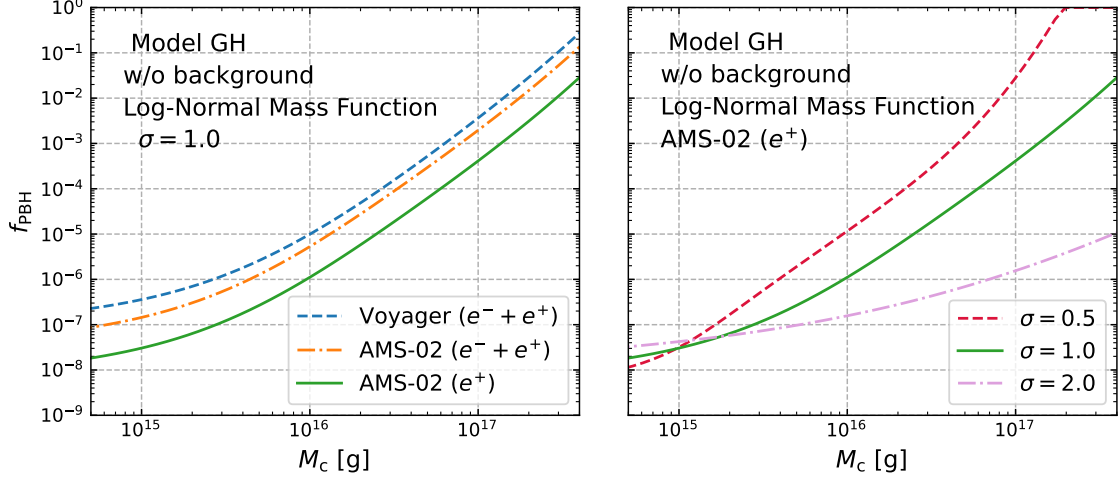


FIG. 5. Left) Constraints on  $f_{\text{PBH}}$  in the GH propagation model with parameters listed in Tab. I. The blue, orange, and green curves represent the constraints obtained individually from the all-electron data of Voyager-1,2 [109], the all-electron data of AMS-02 [110], and the positron data of AMS-02 [110], respectively. The log-normal PBH mass function with width  $\sigma = 1.0$  is assumed. Right) The constraints from the AMS-02 positron data only, for the log-normal PBH mass function with different widths of  $\sigma = 0.5$ , 1.0 and 2.0, respectively.

the same as the evaporation process is charge symmetric. Thus the prediction for all-electron flux from PBH evaporation should be approximately twice the positron flux. However, the all-electron flux measured by AMS-02 is around an order of magnitude higher than of positron flux. Thus the corresponding constraints are significantly weaker in the null background case. The constraints derived in Fig. 4 are in a good agreement with the values previously estimated from the left panel of Fig. 3.

Our analysis also show that value of  $V_a$  plays an important role in constraining  $f_{\text{PBH}}$  from the CR data. As demonstrated in the right panel of Fig. 2, in the case where  $V_a$  is vanishing (model DB), the predicted positron flux exhibits a sharp cutoff at kinetic energies  $\sim 10$  MeV, far below the reach of the AMS-02 experiment. Thus for the DB model, only the constraints can only be obtained from the Voyager all-electron data, as shown in the lower-right panel of Fig 4.

In the left panel of Fig. 5 we show the constraints for log-normally distributed PBHs with a typical width  $\sigma = 1$  in the GH propagation model. Similar to the case with monochromatic mass function, the AMS-02 positron data provide the most stringent limits in the case with log-normal mass function. In the right panel of Fig. 5, the constraints for different widths  $\sigma = 0.5, 1.0$  and  $2.0$  for the log-normal mass function are compared. For the log-normal mass function constraints becomes more stringent as the value of  $\sigma$  increases, which is consistent with the flux predictions in the right panel of Fig. 3.

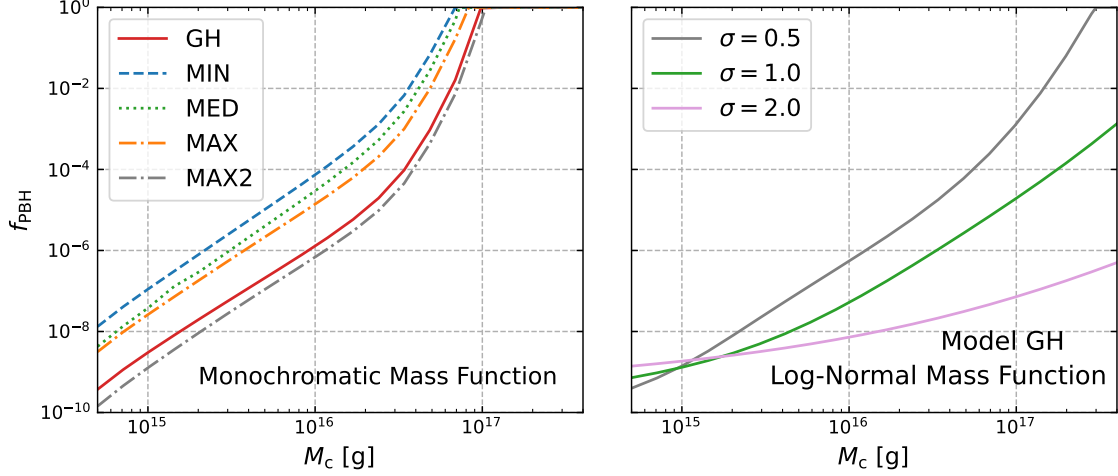


FIG. 6. Left) Constraints on  $f_{\text{PBH}}$  from the AMS-02 positron data with the inclusion of astrophysical backgrounds in five CR propagation models. The PBH mass function is assumed to be monochromatic. Right) The constraints for the log-normal PBH mass function with different widths  $\sigma = 0.5, 1.0, 2.0$  in the GH propagation model.

## B. Constraints with including astrophysical backgrounds

In the next step, we consider the CR-positron constraints including the secondary positron backgrounds. Including the astrophysical background in general results in more stringent constraints. However, so far the theoretical predictions for low-energy (sub-GeV) positron flux still suffer from significant uncertainties. In addition to the uncertainties in propagation models such as the diffusion halo half-height  $z_h$ , large uncertainties arise from the low-energy  $pp$  and  $pA$  inelastic scattering cross sections for positron production. At present, the cross sections are obtained either from analytical parameterizations to the experimental data [111–113] or from QCD-based Monte-Carlo event generators [114–116]. The differences between the approaches are significant. Other uncertainties specifically related to CR electron and positron energy loss involve that in the Galactic magnetic fields and gas distribution (for recently analyses, see e.g. [114, 117]). Due to these uncertainties, the derived constraints including the astrophysical backgrounds are less robust compared with that without backgrounds.

To account for the uncertainties in the secondary positron flux, we introduce two additional free parameters  $N_{e+}$  and  $\delta_{e+}$  into the calculation of the CR positron flux  $\Phi_{e+}$ , namely,  $\Phi_{e+}(E_{\text{kin}}) \rightarrow N_{e+}(E_{\text{kin}}/\text{GeV})^{\delta_{e+}} \Phi_{e+}(E_{\text{kin}})$ . The parameters are determined through fitting to the experimental data. In the presence of backgrounds, we derive the constraints on  $f_{\text{PBH}}$  using the standard minimal- $\chi^2$  approach. For a given mass function parameters of  $M_c$  or a pair of  $(M_c, \sigma)$ , we first find the best-fit parameters  $(\hat{f}_{\text{PBH}}, \hat{N}_{e+}, \hat{\delta}_{e+})$  and the corresponding minimal value of  $\chi^2_{\text{min}}(\hat{f}_{\text{PBH}}, \hat{N}_{e+}, \hat{\delta}_{e+})$ . Then, we increase the value of  $f_{\text{PBH}}$  and repeat the fitting process with respect to the other parameters  $N_{e+}, \delta_{e+}$  and obtain larger values of  $\chi^2$ . This process is repeated until a particular

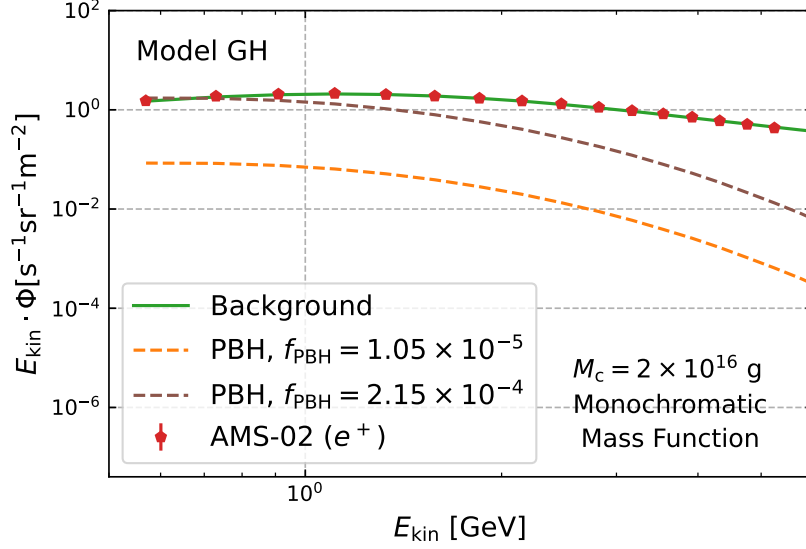


FIG. 7. Secondary background positron fluxes (solid green) and primary positron fluxes from PBH evaporation (dashed orange) corresponding to the derived constraints of  $f_{\text{PBH}} \leq 1.05 \times 10^{-5}$  at 95% C.L. at  $M_c = 2 \times 10^{16}$  g (from Fig. 6) in the GH model. The PBH positron fluxes corresponding to the constraints of  $f_{\text{PBH}} \leq 2.15 \times 10^{-4}$  without including the secondary backgrounds (dashed brown) from Fig. 4 are also shown for comparison purpose.

$f_{\text{PBH}}$  satisfying  $\Delta\chi^2 = \chi^2(f_{\text{PBH}}, \hat{\hat{N}}_{e+}(f_{\text{PBH}}), \hat{\hat{\delta}}_{e+}(f_{\text{PBH}})) - \chi^2_{\min}(\hat{f}_{\text{PBH}}, \hat{N}_{e+}, \hat{\delta}_{e+}) = 3.84$  is found. Here, the parameters with a double hat minimized the  $\chi^2$  function for the given  $f_{\text{PBH}}$ . The obtained values of  $f_{\text{PBH}}$  correspond to the upper limits at the 95% C.L.. The AMS-02 positron flux data in the low-energy region 0.5 – 5.2 GeV (16 data points in total) are included in the data analysis process.

In the left panel of Fig. 6, we show the obtained constraints on  $f_{\text{PBH}}$  as a function of  $M_c$  in the case of monochromatic mass function in five propagation models. The difference between different propagation models are typically within two orders of magnitude. In the GH model,  $\chi^2$  fitting gives  $\hat{f}_{\text{PBH}} = 0$ ,  $\hat{N}_{e+} = 0.255$ , and  $\hat{\delta}_{e+} = 0.995$  with  $\chi^2_{\min}/\text{d.o.f} = 32.51/14$ . Similar results are found for the MAX2 model. For the model MIN-MAX, the constraints are relatively weaker due to the fact that non-vanishing  $\hat{f}_{\text{PBH}}$  are favored. The DB model is not considered in the analysis as the predicted positron energies from this model are too low to be constrained by the AMS-02 data. In the right panel of Fig. 6, the constraints for the log-normal mass function with three width  $\sigma = 0.5, 1.0$  and  $2.0$  in the GH propagation model are shown. Similar to the right panel of Fig. 5, increasing  $\sigma$  leads to more stringent constraints. In all the re-acceleration propagation models, we have verified that the constraints from the low-energy AMS-02 positron data are always the most stringent compared with that from the AMS-02 all-electron or the Voyager-1,2 all-electron data.

Including the secondary CR positron backgrounds can significantly improve the constraints on  $f_{\text{PBH}}$ , if the model of the secondaries agrees with the data well. In Fig. 7, we show the calculated

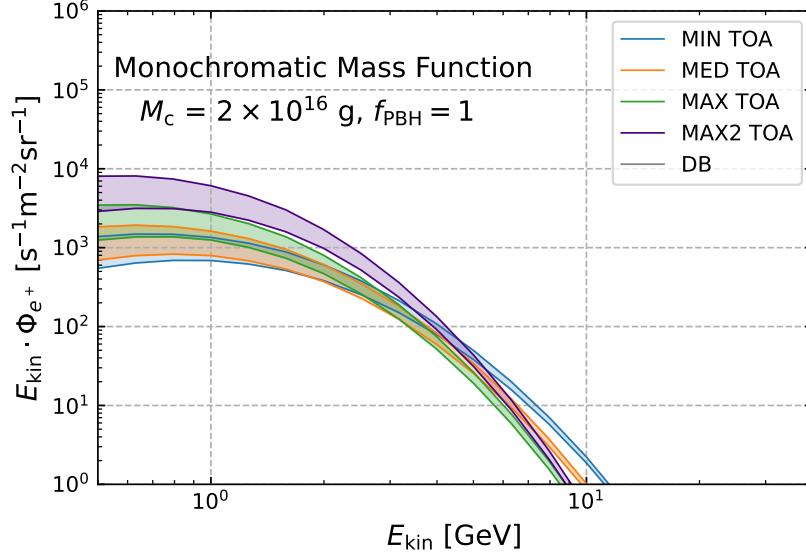


FIG. 8. PBH evaporating positron fluxes at TOA in propagation model MIN, MED, MAX and MAX2. The shaded region represents the uncertainty in the positron flux stemmed from the uncertainty of Fisk potential. The abundance and mass function of PBHs is consistent with the scenario depicted in the right panel of Fig. 2.

secondary positron fluxes correspond to  $M_c = 2 \times 10^{16} \text{ g}$  and  $f_{\text{PBH}} = 1.05 \times 10^{-5}$  (the value allowed at 95% C.L. from Fig. 6) in the GH model. It can be seen that the AMS-02 data can be well-fitted by the secondary positron background, which leads to more stringent constraints. While in the analysis assuming no background, the constraints is around  $f_{\text{PBH}} = 2.15 \times 10^{-4}$  (according to Fig. 4) which is around an order of magnitude weaker.

The uncertainties in modeling the solar modulation effect is an important source of the uncertainties of the obtained constraints, as they mainly affect the low-energy CR fluxes at GeV region. In order to estimate the uncertainties related to the solar modulation effect, we calculate the CR fluxes in the MIN, MED and MAX models with the Fisk potential varying around the default  $\phi_F$  values in Table I by  $\phi \rightarrow \phi_F \pm \Delta\phi_F$ , where  $\Delta\phi_F$  represents the uncertainty in  $\phi_F$  with a typical value of  $\Delta\phi = 0.1 \text{ GV}$ . The results are shown in Fig. 8. It can be seen that the typical uncertainties at  $E_{\text{kin}} \sim 0.5 \text{ GeV}$  which is the lowest positron energy measured by the AMS-02 experiment are around a factor of two for all the models. In Fig. 8, the BD model is not considered as the predicted positron kinetic energies in this model are too low to be observed at TOA, which is consistent with the definition of the force field in Eq. (15).

In Fig. 9, we compare the constraints from the AMS-02 positron data obtained in the GH model with a selection of constraints from other observables such as that from the extragalactic  $\gamma$ -ray [28], CMB [32], 511 keV  $\gamma$ -ray data [39]. The results in [39] considered latitude profile of the 511 keV emission and assumed a NFW DM density profile with an inner slop  $\gamma = 1.6$ . An alternative analysis using longitude emission profile to set constraints on  $f_{\text{PBH}}$  can be found in [40].

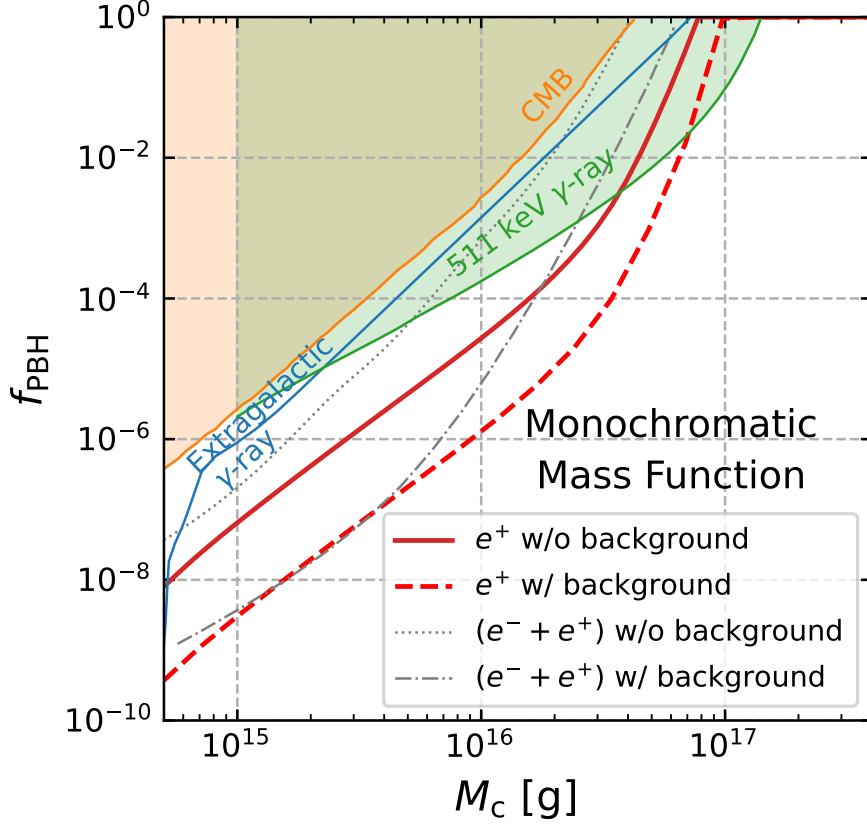


FIG. 9. Exclusion lines of PBHs abundance  $f_{\text{PBH}}$ . Shadow regions are obtained from different observable, including extragalactic  $\gamma$ -rays [28], 511 keV  $\gamma$ -rays data [39], CMB [32]. The 511 keV constraint is derived from a generalized NFW profile incorporating an additional parameter, specifically an inner slope of  $\gamma = 1.6$ . The dotted and dot-dashed lines are the exclusion lines originally obtained in Ref. [37]. The red-solid and red-dashed lines are the results of this work with the employments of model GH and monochromatic mass function, corresponding to the case of including and neglecting CR background, respectively.

In Fig. 9, we also compare our results with that previously obtained from the Voyager-1 all-electron data in a diffusive-reacceleration propagation model (model A) in Ref. [37]. The figure shows that the constraints from AMS-02 positron data are competitive with all these previously obtained constraints, and more stringent than that from the Voyager all-electron data in both the cases with and without including the astrophysical backgrounds.

## V. CONCLUSIONS

In summary, in this work we have explored the possibility of using the low-energy CR positron data to constrain the abundance of primordial black holes. The advantage of using the CR positron data is based on its secondary origin and thus sensitive to any exotic contributions. We have shown that in some typical diffusive re-acceleration CR propagation models, the current

AMS-02 data can place stringent constraints on  $f_{\text{PBH}}$ . As an example, we have shown that in the Galprop+Helmod model for CR propagation in the Galaxy and heliosphere, a conservative upper limit of  $f_{\text{PBH}} \lesssim 2.15 \times 10^{-4}$  at  $M_c = 2 \times 10^{16}$  g can be obtained, which improves the previous constraints from the Voyager-1 data of all-electrons by around an order of magnitude. Admittedly, the main results of this work is obtained for diffusive re-acceleration models with typical  $V_a \sim 30$  km/s which is supported by a number of analysis [46–53], but not yet conclusive. Compared with other observables such as diffusive  $\gamma$ -rays, using the CR flux data to constrain PBH abundance in general suffers from uncertainties in the propagation models, which are expected to be improved in the future with more precise CR data. For models without re-acceleration, the AMS-02 constraints are not applicable as shown in Fig. 4, which underscores the necessity of complementary probes such as gamma-ray surveys and synchrotron radiations to constrain PBH scenarios.

**Note added:** After submitting the manuscript to arXiv, we were aware of a similar paper arXiv:2403.04988. Their major conclusions are in agreement with this work.

## ACKNOWLEDGMENTS

This work is supported in part by the NSFC under Grants No. 11825506, No. 11821505, and No. 12441504.

- 
- [1] M. Bauer and T. Plehn, *Yet Another Introduction to Dark Matter: The Particle Physics Approach*, vol. 959 of *Lecture Notes in Physics*. Springer, 2019. [arXiv:1705.01987 \[hep-ph\]](#).
  - [2] K. N. Abazajian *et al.*, “Light Sterile Neutrinos: A White Paper,” [arXiv:1204.5379 \[hep-ph\]](#).
  - [3] D. J. E. Marsh, “Axion Cosmology,” *Phys. Rept.* **643** (2016) 1–79, [arXiv:1510.07633 \[astro-ph.CO\]](#).
  - [4] S. Hawking, “Gravitationally collapsed objects of very low mass,” *Mon. Not. Roy. Astron. Soc.* **152** (1971) 75.
  - [5] B. J. Carr and S. W. Hawking, “Black holes in the early Universe,” *Mon. Not. Roy. Astron. Soc.* **168** (1974) 399–415.
  - [6] H. Tashiro and N. Sugiyama, “Constraints on Primordial Black Holes by Distortions of Cosmic Microwave Background,” *Phys. Rev. D* **78** (2008) 023004, [arXiv:0801.3172 \[astro-ph\]](#).
  - [7] C. Germani and I. Musco, “Abundance of Primordial Black Holes Depends on the Shape of the Inflationary Power Spectrum,” *Phys. Rev. Lett.* **122** no. 14, (2019) 141302, [arXiv:1805.04087 \[astro-ph.CO\]](#).
  - [8] K. Kannike, L. Marzola, M. Raidal, and H. Veermäe, “Single Field Double Inflation and Primordial Black Holes,” *JCAP* **09** (2017) 020, [arXiv:1705.06225 \[astro-ph.CO\]](#).

- [9] B. Carr, M. Raidal, T. Tenkanen, V. Vaskonen, and H. Veermäe, “Primordial black hole constraints for extended mass functions,” *Phys. Rev. D* **96** no. 2, (2017) 023514, [arXiv:1705.05567 \[astro-ph.CO\]](#).
- [10] B. Carr, T. Tenkanen, and V. Vaskonen, “Primordial black holes from inflaton and spectator field perturbations in a matter-dominated era,” *Phys. Rev. D* **96** no. 6, (2017) 063507, [arXiv:1706.03746 \[astro-ph.CO\]](#).
- [11] **MACHO** Collaboration, C. Alcock *et al.*, “The MACHO project: Microlensing results from 5.7 years of LMC observations,” *Astrophys. J.* **542** (2000) 281–307, [arXiv:astro-ph/0001272](#).
- [12] L. Wyrzykowski *et al.*, “The OGLE View of Microlensing towards the Magellanic Clouds. III. Ruling out sub-solar MACHOs with the OGLE-III LMC data,” *Mon. Not. Roy. Astron. Soc.* **413** (2011) 493, [arXiv:1012.1154 \[astro-ph.GA\]](#).
- [13] L. Wyrzykowski *et al.*, “The OGLE View of Microlensing towards the Magellanic Clouds. IV. OGLE-III SMC Data and Final Conclusions on MACHOs,” *Mon. Not. Roy. Astron. Soc.* **416** (2011) 2949, [arXiv:1106.2925 \[astro-ph.GA\]](#).
- [14] **Macho** Collaboration, R. A. Allsman *et al.*, “MACHO project limits on black hole dark matter in the 1-30 solar mass range,” *Astrophys. J. Lett.* **550** (2001) L169, [arXiv:astro-ph/0011506](#).
- [15] K. Griest, A. M. Cieplak, and M. J. Lehner, “Experimental Limits on Primordial Black Hole Dark Matter from the First 2 yr of Kepler Data,” *Astrophys. J.* **786** no. 2, (2014) 158, [arXiv:1307.5798 \[astro-ph.CO\]](#).
- [16] S. Calchi Novati, S. Mirzoyan, P. Jetzer, and G. Scarpetta, “Microlensing towards the SMC: a new analysis of OGLE and EROS results,” *Mon. Not. Roy. Astron. Soc.* **435** (2013) 1582, [arXiv:1308.4281 \[astro-ph.GA\]](#).
- [17] K. Griest, A. M. Cieplak, and M. J. Lehner, “New Limits on Primordial Black Hole Dark Matter from an Analysis of Kepler Source Microlensing Data,” *Phys. Rev. Lett.* **111** no. 18, (2013) 181302.
- [18] S. M. Koushiappas and A. Loeb, “Dynamics of Dwarf Galaxies Disfavor Stellar-Mass Black Holes as Dark Matter,” *Phys. Rev. Lett.* **119** no. 4, (2017) 041102, [arXiv:1704.01668 \[astro-ph.GA\]](#).
- [19] M. A. Monroy-Rodríguez and C. Allen, “The end of the MACHO era- revisited: new limits on MACHO masses from halo wide binaries,” *Astrophys. J.* **790** no. 2, (2014) 159, [arXiv:1406.5169 \[astro-ph.GA\]](#).
- [20] B. Carr, “Primordial black holes as dark matter and generators of cosmic structure,” *Astrophys. Space Sci. Proc.* **56** (2019) 29–39, [arXiv:1901.07803 \[astro-ph.CO\]](#).
- [21] **MUSE** Collaboration, S. L. Zoutendijk *et al.*, “The MUSE-Faint survey: I. Spectroscopic evidence for a star cluster in Eridanus 2 and constraints on MACHOs as a constituent of dark matter,” *Astron. Astrophys.* **635** (2020) A107, [arXiv:2001.08790 \[astro-ph.GA\]](#).
- [22] B. Carr, K. Kohri, Y. Sendouda, and J. Yokoyama, “Constraints on primordial black holes,” *Rept. Prog. Phys.* **84** no. 11, (2021) 116902, [arXiv:2002.12778 \[astro-ph.CO\]](#).
- [23] B. Carr and F. Kuhnel, “Primordial Black Holes as Dark Matter: Recent Developments,” *Ann. Rev. Nucl. Part. Sci.* **70** (2020) 355–394, [arXiv:2006.02838 \[astro-ph.CO\]](#).



- [24] S. W. Hawking, “Black hole explosions,” *Nature* **248** (1974) 30–31.
- [25] I. Baldes, Q. Decant, D. C. Hooper, and L. Lopez-Honorez, “Non-Cold Dark Matter from Primordial Black Hole Evaporation,” *JCAP* **08** (2020) 045, [arXiv:2004.14773 \[astro-ph.CO\]](#).
- [26] A. Cheek, L. Heurtier, Y. F. Perez-Gonzalez, and J. Turner, “Primordial black hole evaporation and dark matter production. I. Solely Hawking radiation,” *Phys. Rev. D* **105** no. 1, (2022) 015022, [arXiv:2107.00013 \[hep-ph\]](#).
- [27] J. H. MacGibbon, “Quark and gluon jet emission from primordial black holes. 2. The Lifetime emission,” *Phys. Rev. D* **44** (1991) 376–392.
- [28] B. J. Carr, K. Kohri, Y. Sendouda, and J. Yokoyama, “New cosmological constraints on primordial black holes,” *Phys. Rev. D* **81** (2010) 104019, [arXiv:0912.5297 \[astro-ph.CO\]](#).
- [29] B. J. Carr, K. Kohri, Y. Sendouda, and J. Yokoyama, “Constraints on primordial black holes from the Galactic gamma-ray background,” *Phys. Rev. D* **94** no. 4, (2016) 044029, [arXiv:1604.05349 \[astro-ph.CO\]](#).
- [30] A. Arbey, J. Auffinger, and J. Silk, “Constraining primordial black hole masses with the isotropic gamma ray background,” *Phys. Rev. D* **101** no. 2, (2020) 023010, [arXiv:1906.04750 \[astro-ph.CO\]](#).
- [31] R. Laha, J. B. Muñoz, and T. R. Slatyer, “INTEGRAL constraints on primordial black holes and particle dark matter,” *Phys. Rev. D* **101** no. 12, (2020) 123514, [arXiv:2004.00627 \[astro-ph.CO\]](#).
- [32] J. Auffinger, “Primordial black hole constraints with Hawking radiation—A review,” *Prog. Part. Nucl. Phys.* **131** (2023) 104040, [arXiv:2206.02672 \[astro-ph.CO\]](#).
- [33] B. Dasgupta, R. Laha, and A. Ray, “Neutrino and positron constraints on spinning primordial black hole dark matter,” *Phys. Rev. Lett.* **125** no. 10, (2020) 101101, [arXiv:1912.01014 \[hep-ph\]](#).
- [34] S. Wang, D.-M. Xia, X. Zhang, S. Zhou, and Z. Chang, “Constraining primordial black holes as dark matter at JUNO,” *Phys. Rev. D* **103** no. 4, (2021) 043010, [arXiv:2010.16053 \[hep-ph\]](#).
- [35] N. Bernal, V. Muñoz Alborno, S. Palomares-Ruiz, and P. Villanueva-Domingo, “Current and future neutrino limits on the abundance of primordial black holes,” *JCAP* **10** (2022) 068, [arXiv:2203.14979 \[hep-ph\]](#).
- [36] Q. Liu and K. C. Y. Ng, “The Sensitivity Floor for Primordial Black Holes with Neutrino Searches,” [arXiv:2312.06108 \[hep-ph\]](#).
- [37] M. Boudaud and M. Cirelli, “Voyager 1  $e^\pm$  Further Constrain Primordial Black Holes as Dark Matter,” *Phys. Rev. Lett.* **122** no. 4, (2019) 041104, [arXiv:1807.03075 \[astro-ph.HE\]](#).
- [38] R. Laha, “Primordial Black Holes as a Dark Matter Candidate Are Severely Constrained by the Galactic Center 511 keV  $\gamma$ -Ray Line,” *Phys. Rev. Lett.* **123** no. 25, (2019) 251101, [arXiv:1906.09994 \[astro-ph.HE\]](#).
- [39] C. Keith and D. Hooper, “511 keV excess and primordial black holes,” *Phys. Rev. D* **104** no. 6, (2021) 063033, [arXiv:2103.08611 \[astro-ph.CO\]](#).
- [40] P. D. la Torre Luque, J. Koechler, and S. Balaji, “Refining galactic primordial black hole evaporation

- constraints,” 2024. <https://arxiv.org/abs/2406.11949>.
- [41] S. Mittal, A. Ray, G. Kulkarni, and B. Dasgupta, “Constraining primordial black holes as dark matter using the global 21-cm signal with X-ray heating and excess radio background,” *JCAP* **03** (2022) 030, [arXiv:2107.02190](https://arxiv.org/abs/2107.02190) [astro-ph.CO].
  - [42] K. Maki, T. Mitsui, and S. Orito, “Local flux of low-energy anti-protons from evaporating primordial black holes,” *Phys. Rev. Lett.* **76** (1996) 3474–3477, [arXiv:astro-ph/9601025](https://arxiv.org/abs/astro-ph/9601025).
  - [43] A. Barrau, G. Boudoul, F. Donato, D. Maurin, P. Salati, and R. Taillet, “Anti-protons from primordial black holes,” *Astron. Astrophys.* **388** (2002) 676, [arXiv:astro-ph/0112486](https://arxiv.org/abs/astro-ph/0112486).
  - [44] H.-B. Jin, Y.-L. Wu, and Y.-F. Zhou, “Astrophysical background and dark matter implication based on latest AMS-02 data,” *Astrophys. J.* **901** no. 1, (2020) 80, [arXiv:1701.02213](https://arxiv.org/abs/1701.02213) [hep-ph].
  - [45] V. S. Berezinsky, S. V. Bulanov, V. A. Dogiel, and V. S. Ptuskin, *Astrophysics of cosmic rays*. Springer Berlin, Heidelberg, 1990.
  - [46] R. Trotta, G. Jóhannesson, I. V. Moskalenko, T. A. Porter, R. R. d. Austri, and A. W. Strong, “Constraints on cosmic-ray propagation models from a global Bayesian analysis,” *Astrophys. J.* **729** (2011) 106, [arXiv:1011.0037](https://arxiv.org/abs/1011.0037) [astro-ph.HE].
  - [47] H.-B. Jin, Y.-L. Wu, and Y.-F. Zhou, “Cosmic ray propagation and dark matter in light of the latest AMS-02 data,” *JCAP* **09** (2015) 049, [arXiv:1410.0171](https://arxiv.org/abs/1410.0171) [hep-ph].
  - [48] Q. Yuan, C.-R. Zhu, X.-J. Bi, and D.-M. Wei, “Secondary cosmic-ray nucleus spectra disfavor particle transport in the Galaxy without reacceleration,” *JCAP* **11** (2020GV) 027, [arXiv:1810.03141](https://arxiv.org/abs/1810.03141) [astro-ph.HE].
  - [49] M. J. Boschini *et al.*, “Solution of heliospheric propagation: unveiling the local interstellar spectra of cosmic ray species,” *Astrophys. J.* **840** no. 2, (2017) 115, [arXiv:1704.06337](https://arxiv.org/abs/1704.06337) [astro-ph.HE].
  - [50] M. J. Boschini *et al.*, “Deciphering the local Interstellar spectra of secondary nuclei with GALPROP/HelMod framework and a hint for primary lithium in cosmic rays,” *Astrophys. J.* **889** (2020) 167, [arXiv:1911.03108](https://arxiv.org/abs/1911.03108) [astro-ph.HE].
  - [51] M. J. Boschini *et al.*, “Inference of the Local Interstellar Spectra of Cosmic-Ray Nuclei  $Z \leq 28$  with the GalProp–HelMod Framework,” *Astrophys. J. Suppl.* **250** no. 2, (2020) 27, [arXiv:2006.01337](https://arxiv.org/abs/2006.01337) [astro-ph.HE].
  - [52] P. De La Torre Luque, M. N. Mazziotta, F. Loparco, F. Gargano, and D. Serini, “Implications of current nuclear cross sections on secondary cosmic rays with the upcoming DRAGON2 code,” *JCAP* **03** (2021) 099, [arXiv:2101.01547](https://arxiv.org/abs/2101.01547) [astro-ph.HE].
  - [53] P. D. L. T. Luque, M. N. Mazziotta, F. Loparco, F. Gargano, and D. Serini, “Markov chain Monte Carlo analyses of the flux ratios of B, Be and Li with the DRAGON2 code,” *JCAP* **07** (2021) 010, [arXiv:2102.13238](https://arxiv.org/abs/2102.13238) [astro-ph.HE].
  - [54] P. De la Torre Luque, S. Balaji, and P. Carenza, “Multimessenger search for electrophilic feebly interacting particles from supernovae,” *Phys. Rev. D* **109** no. 10, (2024) 103028, [arXiv:2307.13731](https://arxiv.org/abs/2307.13731) [hep-ph].
  - [55] P. De la Torre Luque, S. Balaji, and P. Carenza, “Robust constraints on feebly interacting particles

- using XMM-Newton,” *Phys. Rev. D* **109** no. 10, (2024) L101305, [arXiv:2307.13728 \[hep-ph\]](#).
- [56] P. De la Torre Luque, S. Balaji, and J. Koechler, “Importance of Cosmic-Ray Propagation on Sub-GeV Dark Matter Constraints,” *Astrophys. J.* **968** no. 1, (2024) 46, [arXiv:2311.04979 \[hep-ph\]](#).
- [57] P. De la Torre Luque, S. Balaji, and J. Silk, “New 511 keV line data provides strongest sub-GeV dark matter constraints,” [arXiv:2312.04907 \[hep-ph\]](#).
- [58] A. W. Strong and I. V. Moskalenko, “Propagation of cosmic-ray nucleons in the galaxy,” *Astrophys. J.* **509** (1998) 212–228, [arXiv:astro-ph/9807150](#).
- [59] I. V. Moskalenko, A. W. Strong, J. F. Ormes, and M. S. Potgieter, “Secondary anti-protons and propagation of cosmic rays in the galaxy and heliosphere,” *Astrophys. J.* **565** (2002) 280–296, [arXiv:astro-ph/0106567](#).
- [60] A. W. Strong and I. V. Moskalenko, “Models for galactic cosmic ray propagation,” *Adv. Space Res.* **27** (2001) 717–726, [arXiv:astro-ph/0101068](#).
- [61] I. V. Moskalenko, A. W. Strong, S. G. Mashnik, and J. F. Ormes, “Challenging cosmic ray propagation with antiprotons. Evidence for a fresh nuclei component?,” *Astrophys. J.* **586** (2003) 1050–1066, [arXiv:astro-ph/0210480](#).
- [62] V. S. Ptuskin, I. V. Moskalenko, F. C. Jones, A. W. Strong, and V. N. Zirakashvili, “Dissipation of magnetohydrodynamic waves on energetic particles: impact on interstellar turbulence and cosmic ray transport,” *Astrophys. J.* **642** (2006) 902–916, [arXiv:astro-ph/0510335](#).
- [63] P. Bobik *et al.*, “Systematic Investigation of Solar Modulation of Galactic Protons for Solar Cycle 23 using a Monte Carlo Approach with Particle Drift Effects and Latitudinal Dependence,” *Astrophys. J.* **745** (2012) 132, [arXiv:1110.4315 \[astro-ph.SR\]](#).
- [64] P. Bobik, M. J. Boschini, S. Della Torre, M. Gervasi, D. Grandi, G. La Vacca, S. Pensotti, M. Putis, P. G. Rancoita, D. Rozza, M. Tacconi, and M. Zannoni, “On the forward-backward-in-time approach for monte carlo solution of parker’s transport equation: One-dimensional case,” *Journal of Geophysical Research: Space Physics* **121** no. 5, (2016) 3920–3930.
- [65] M. J. Boschini, S. Della Torre, M. Gervasi, G. La Vacca, and P. G. Rancoita, “Propagation of cosmic rays in heliosphere: The HELMOD model,” *Adv. Space Res.* **62** (2018) 2859–2879, [arXiv:1704.03733 \[astro-ph.SR\]](#).
- [66] M. J. Boschini, S. Della Torre, M. Gervasi, G. La Vacca, and P. G. Rancoita, “The HelMod Model in the Works for Inner and Outer Heliosphere: from AMS to Voyager Probes Observations,” *Adv. Space Res.* **64** no. 12, (2019) 2459–2476, [arXiv:1903.07501 \[physics.space-ph\]](#).
- [67] M. J. Boschini, S. Della Torre, M. Gervasi, G. La Vacca, and P. G. Rancoita, “Forecasting of cosmic rays intensities with HelMod Model,” *Adv. Space Res.* **70** no. 9, (2022) 2649–2657.
- [68] J. Auffinger and A. Arbey, “Beyond the Standard Model with BlackHawk v2.0,” *PoS CompTools2021* (2022) 017, [arXiv:2207.03266 \[gr-qc\]](#).
- [69] V. De Luca, V. Desjacques, G. Franciolini, A. Malhotra, and A. Riotto, “The initial spin probability distribution of primordial black holes,” *JCAP* **05** (2019) 018, [arXiv:1903.01179](#)

- [astro-ph.CO].
- [70] T. Chiba and S. Yokoyama, “Spin Distribution of Primordial Black Holes,” *PTEP* **2017** no. 8, (2017) 083E01, [arXiv:1704.06573 \[gr-qc\]](#).
  - [71] M. Mirbabayi, A. Gruzinov, and J. Noreña, “Spin of Primordial Black Holes,” *JCAP* **03** (2020) 017, [arXiv:1901.05963 \[astro-ph.CO\]](#).
  - [72] T. Harada, C.-M. Yoo, K. Kohri, K.-i. Nakao, and S. Jhingan, “Primordial black hole formation in the matter-dominated phase of the Universe,” *Astrophys. J.* **833** no. 1, (2016) 61, [arXiv:1609.01588 \[astro-ph.CO\]](#).
  - [73] T. Harada, C.-M. Yoo, K. Kohri, and K.-I. Nakao, “Spins of primordial black holes formed in the matter-dominated phase of the Universe,” *Phys. Rev. D* **96** no. 8, (2017) 083517, [arXiv:1707.03595 \[gr-qc\]](#). [Erratum: *Phys.Rev.D* 99, 069904 (2019)].
  - [74] E. Cotner and A. Kusenko, “Primordial black holes from scalar field evolution in the early universe,” *Phys. Rev. D* **96** no. 10, (2017) 103002, [arXiv:1706.09003 \[astro-ph.CO\]](#).
  - [75] S. W. Hawking, “Particle Creation by Black Holes,” in *1st Oxford Conference on Quantum Gravity*. 8, 1975.
  - [76] D. N. Page, “Particle Emission Rates from a Black Hole: Massless Particles from an Uncharged, Nonrotating Hole,” *Phys. Rev. D* **13** (1976) 198–206.
  - [77] A. Arbey and J. Auffinger, “BlackHawk: A public code for calculating the Hawking evaporation spectra of any black hole distribution,” *Eur. Phys. J. C* **79** no. 8, (2019) 693, [arXiv:1905.04268 \[gr-qc\]](#).
  - [78] A. Coogan, L. Morrison, and S. Profumo, “Hazma: A Python Toolkit for Studying Indirect Detection of Sub-GeV Dark Matter,” *JCAP* **01** (2020) 056, [arXiv:1907.11846 \[hep-ph\]](#).
  - [79] A. Dolgov and J. Silk, “Baryon isocurvature fluctuations at small scales and baryonic dark matter,” *Phys. Rev. D* **47** (1993) 4244–4255.
  - [80] S. Clesse and J. García-Bellido, “Massive Primordial Black Holes from Hybrid Inflation as Dark Matter and the seeds of Galaxies,” *Phys. Rev. D* **92** no. 2, (2015) 023524, [arXiv:1501.07565 \[astro-ph.CO\]](#).
  - [81] J. H. MacGibbon and B. R. Webber, “Quark and gluon jet emission from primordial black holes: The instantaneous spectra,” *Phys. Rev. D* **41** (1990) 3052–3079.
  - [82] W. Chao, T. Li, and J. Liao, “Connecting Primordial Black Hole to boosted sub-GeV Dark Matter through neutrino,” [arXiv:2108.05608 \[hep-ph\]](#).
  - [83] W. R. Webber, M. A. Lee, and M. Gupta, “Propagation of cosmic-ray nuclei in a diffusing galaxy with convective halo and thin matter disk,” *Astrophys. J.* **390** (1992) 96.
  - [84] A. W. Strong, I. V. Moskalenko, and V. S. Ptuskin, “Cosmic-ray propagation and interactions in the Galaxy,” *Ann. Rev. Nucl. Part. Sci.* **57** (2007) 285–327, [arXiv:astro-ph/0701517](#).
  - [85] A. Kolmogorov, “The Local Structure of Turbulence in Incompressible Viscous Fluid for Very Large Reynolds’ Numbers,” *Akademiia Nauk SSSR Doklady* **30** (Jan., 1941) 301–305.
  - [86] P. S. Iroshnikov, “Turbulence of a Conducting Fluid in a Strong Magnetic Field,” *Soviet Astronomy*

- 7 (Feb., 1964) 566.
- [87] R. H. Kraichnan, “Inertial-Range Spectrum of Hydromagnetic Turbulence,” *The Physics of Fluids* **8** no. 7, (07, 1965) 1385–1387, [https://pubs.aip.org/aip/pfl/article-pdf/8/7/1385/12617184/1385\\_1\\_online.pdf](https://pubs.aip.org/aip/pfl/article-pdf/8/7/1385/12617184/1385_1_online.pdf). <https://doi.org/10.1063/1.1761412>.
  - [88] E. S. Seo and V. S. Ptuskin, “Stochastic Reacceleration of Cosmic Rays in the Interstellar Medium,” *The Astrophysical Journal* **431** (Aug., 1994) 705.
  - [89] D. Maurin, R. Taillet, F. Donato, P. Salati, A. Barrau, and G. Boudoul, “Galactic cosmic ray nuclei as a tool for astroparticle physics,” [arXiv:astro-ph/0212111](https://arxiv.org/abs/astro-ph/0212111).
  - [90] I. V. Moskalenko and A. W. Strong, “Production and propagation of cosmic ray positrons and electrons,” *Astrophys. J.* **493** (1998) 694–707, [arXiv:astro-ph/9710124](https://arxiv.org/abs/astro-ph/9710124).
  - [91] M. A. Gordon and W. B. Burton, “Carbon monoxide in the Galaxy. I. The radial distribution of CO, H<sub>2</sub>, and nucleons,” *Astrophys. J.* **208** (Sept., 1976) 346–353.
  - [92] P. Cox, E. Kruegel, and P. G. Mezger, “Principal heating sources of dust in the galactic disk,” *Astronomy and Astrophysics* **155** (Feb., 1986) 380–396.
  - [93] L. Bronfman, R. S. Cohen, H. Alvarez, J. May, and P. Thaddeus, “A CO Survey of the Southern Milky Way: The Mean Radial Distribution of Molecular Clouds within the Solar Circle,” *Astrophys. J.* **324** (Jan., 1988) 248.
  - [94] J. M. Cordes, J. M. Weisberg, D. A. Frail, S. R. Spangler, and M. Ryan, “The galactic distribution of free electrons,” *Nature (London)* **354** no. 6349, (Nov., 1991) 121–124.
  - [95] T. J. Sodroski, N. Odegard, R. G. Arendt, E. Dwek, J. L. Weiland, M. G. Hauser, and T. Kelsall, “A Three-dimensional Decomposition of the Infrared Emission from Dust in the Milky Way,” *Astrophysical Journal* **480** no. 1, (May, 1997) 173–187.
  - [96] R. Kappl, “SOLARPROP: Charge-sign Dependent Solar Modulation for Everyone,” *Comput. Phys. Commun.* **207** (2016) 386–399, [arXiv:1511.07875](https://arxiv.org/abs/1511.07875) [astro-ph.SR].
  - [97] A. Vittino, C. Evoli, and D. Gaggero, “Cosmic-ray transport in the heliosphere with HelioProp,” *PoS ICRC2017* (2018) 024, [arXiv:1707.09003](https://arxiv.org/abs/1707.09003) [astro-ph.HE].
  - [98] L. J. Gleeson and W. I. Axford, “Solar Modulation of Galactic Cosmic Rays,” *Astrophys. J.* **154** (1968) 1011.
  - [99] M. Simon and U. Heinbach, “Production of anti-protons in interstellar space by propagating cosmic rays under conditions of diffusive reacceleration,” *Astrophys. J.* **456** (1996) 519–524.
  - [100] G. Jóhannesson *et al.*, “Bayesian analysis of cosmic-ray propagation: evidence against homogeneous diffusion,” *Astrophys. J.* **824** no. 1, (2016) 16, [arXiv:1602.02243](https://arxiv.org/abs/1602.02243) [astro-ph.HE].
  - [101] M. Korsmeier and A. Cuoco, “Implications of Lithium to Oxygen AMS-02 spectra on our understanding of cosmic-ray diffusion,” *Phys. Rev. D* **103** no. 10, (2021) 103016, [arXiv:2103.09824](https://arxiv.org/abs/2103.09824) [astro-ph.HE].
  - [102] Y. Génolini *et al.*, “Cosmic-ray transport from AMS-02 boron to carbon ratio data: Benchmark models and interpretation,” *Phys. Rev. D* **99** no. 12, (2019) 123028, [arXiv:1904.08917](https://arxiv.org/abs/1904.08917)

- [astro-ph.HE].
- [103] N. Weinrich, Y. Génolini, M. Boudaud, L. Derome, and D. Maurin, “Combined analysis of AMS-02 (Li,Be,B)/C, N/O, 3He, and 4He data,” *Astron. Astrophys.* **639** (2020) A131, [arXiv:2002.11406 \[astro-ph.HE\]](#).
- [104] E. Orlando and A. Strong, “Galactic synchrotron emission with cosmic ray propagation models,” *Mon. Not. Roy. Astron. Soc.* **436** (2013) 2127, [arXiv:1309.2947 \[astro-ph.GA\]](#).
- [105] A. Neronov, D. V. Semikoz, and A. M. Taylor, “Low-energy break in the spectrum of Galactic cosmic rays,” *Phys. Rev. Lett.* **108** (2012) 051105, [arXiv:1112.5541 \[astro-ph.HE\]](#).
- [106] M. J. Boschini *et al.*, “HelMod in the works: from direct observations to the local interstellar spectrum of cosmic-ray electrons,” *Astrophys. J.* **854** no. 2, (2018) 94, [arXiv:1801.04059 \[astro-ph.HE\]](#).
- [107] AMS Collaboration, M. Aguilar *et al.*, “Properties of Cosmic-Ray Sulfur and Determination of the Composition of Primary Cosmic-Ray Carbon, Neon, Magnesium, and Sulfur: Ten-Year Results from the Alpha Magnetic Spectrometer,” *Phys. Rev. Lett.* **130** no. 21, (2023) 211002.
- [108] J. F. Navarro, C. S. Frenk, and S. D. M. White, “A Universal density profile from hierarchical clustering,” *Astrophys. J.* **490** (1997) 493–508, [arXiv:astro-ph/9611107](#).
- [109] E. Stone, A. Cummings, and B. Heikkilä, “Cosmic ray measurements from voyager 2 as it crossed into interstellar space,” *Nature Astronomy* **3** (11, 2019) 1013–1018.
- [110] AMS Collaboration, M. Aguilar *et al.*, “The Alpha Magnetic Spectrometer (AMS) on the international space station: Part II — Results from the first seven years,” *Phys. Rept.* **894** (2021) 1–116.
- [111] L. Orusa, M. Di Mauro, F. Donato, and M. Korsmeier, “New determination of the production cross section for secondary positrons and electrons in the Galaxy,” *Phys. Rev. D* **105** no. 12, (2022) 123021, [arXiv:2203.13143 \[astro-ph.HE\]](#).
- [112] E. Kafexhiu, F. Aharonian, A. M. Taylor, and G. S. Vila, “Parametrization of gamma-ray production cross-sections for pp interactions in a broad proton energy range from the kinematic threshold to PeV energies,” *Phys. Rev. D* **90** no. 12, (2014) 123014, [arXiv:1406.7369 \[astro-ph.HE\]](#).
- [113] T. Kamae, N. Karlsson, T. Mizuno, T. Abe, and T. Koi, “Parameterization of Gamma, e $\pm$  and Neutrino Spectra Produced by p-p Interaction in Astronomical Environment,” *Astrophys. J.* **647** (2006) 692–708, [arXiv:astro-ph/0605581](#). [Erratum: *Astrophys.J.* 662, 779 (2007)].
- [114] P. De la Torre Luque, F. Loparco, and M. N. Mazziotta, “The FLUKA cross sections for cosmic-ray leptons and uncertainties on current positron predictions,” *JCAP* **10** (2023) 011, [arXiv:2305.02958 \[astro-ph.HE\]](#).
- [115] S. Koldobskiy, M. Kachelrieß, A. Lskavyan, A. Neronov, S. Ostapchenko, and D. V. Semikoz, “Energy spectra of secondaries in proton-proton interactions,” *Phys. Rev. D* **104** no. 12, (2021) 123027, [arXiv:2110.00496 \[astro-ph.HE\]](#).
- [116] C. Bierlich *et al.*, “A comprehensive guide to the physics and usage of PYTHIA 8.3,” *SciPost Phys. Codeb.* **2022** (2022) 8, [arXiv:2203.11601 \[hep-ph\]](#).

- [117] M. Di Mauro, F. Donato, M. Korsmeier, S. Manconi, and L. Orusa, “Novel prediction for secondary positrons and electrons in the Galaxy,” *Phys. Rev. D* **108** no. 6, (2023) 063024, [arXiv:2304.01261 \[astro-ph.HE\]](#).